remote sensing

MDPI

Article

Irrigation Cooling Effect on Local Temperatures in the North China Plain Based on an Improved Detection Method

Mengjie Hou, Lin Zhao and Aiwen Lin *

School of Resource and Environmental Science, Wuhan University, Wuhan 430079, China; houmengjie@whu.edu.cn (M.H.); linzhao@whu.edu.cn (L.Z.)
* Correspondence: awlin@whu.edu.cn

Abstract: Irrigation has excellent potential for altering surface characteristics and the local climate. Although studies using site observations or remote sensing data have demonstrated an irrigation cooling effect (ICE) on the air temperature (Tem) and land surface temperature (LST), it is difficult to eliminate other stress factors due to different backgrounds. We characterized the irrigation effect as the differences (Δ) of LST and DCT (DCT = LST − Tem) between irrigated and adjacent non-irrigated areas. An improved method was proposed to detect it over the North China Plain (NCP) based on satellite observations. We also investigated the effects of irrigation on Tem, precipitation, NDVI, and ET, and explored the relationships between them. The results show that irrigation induced a decrease in the daytime/nighttime LST and DCT (−0.13/−0.09 and −0.14/−0.07 °C yr^{-1}), Tem (−0.023 °C in spring), and precipitation (−1.461 mm yr^{-1}), and an increase in NDVI (0.03 in spring) and ET (0.289 mm yr^{-1}) across the NCP. The effect on nighttime LST and NDVI increased by 0.04 °C 10 yr^{-1} and 0.003 10 yr^{-1}, and that on ET weakened by 0.23 mm 10 yr^{-1} during 2000–2015. The ICE on the LST had evident spatiotemporal heterogeneity, which was greater in the daytime, in the spring, and in the northern area of the NCP (dry–hot conditions). The daytime ICE in the NCP and northern NCP was 0.37 and 0.50 °C during spring, respectively, with the strongest ICE of 0.60 °C in Henan; however, the ICE was less evident (<0.1 °C) in the southern NCP throughout the year. The ΔNDVI, ΔET, and ΔTem were the main factors driving ICE, explaining approximatively 22%, 45%, and 25% of the daytime ICE, respectively. For every unit of these measures that was increased, the daytime ICE increased by about 7.3, 4.6, and 1.5 °C, respectively. This study highlights the broad irrigation effect on LST, ET, NDVI, and the climate, and provides important information for predicting climate change in the future. The improved method is more suitable for regions with uneven terrain and a varying climate.

Keywords: irrigation effect; LST; NDVI; ET; climate; North China Plain

check for updates

Citation: Hou, M.; Zhao, L.; Lin, A. Irrigation Cooling Effect on Local Temperatures in the North China Plain Based on an Improved Detection Method. *Remote Sens.* **2023**, *15*, 4571. https://doi.org/10.3390/rs15184571

Academic Editor: Won-Ho Nam

Received: 13 July 2023
Revised: 10 September 2023
Accepted: 15 September 2023
Published: 17 September 2023

Copyright: © 2023 by the authors. Licensee MDPI, Basel, Switzerland. This article is an open access article distributed under the terms and conditions of the Creative Commons Attribution (CC BY) license (https://creativecommons.org/licenses/by/4.0/).

1. Introduction

Irrigation is a considerable adaptation strategy to improve the ability of crops to resist global climate change [1],which is crucial to maintain crop production in water-deficient areas. Irrigation water can benefit crops by meeting their water demand; in addition, it can also mitigate crop heat stress through the cooling produced by evaporation [2]. Globally, agricultural irrigation accounts for about 70% of freshwater withdrawals and 90% of consumption [3–5], and irrigated agriculture produces 40% of the grain yield [6]. Moreover, irrigation also constitutes an artificial land-use change [7]; therefore, irrigation is considered to be the most extensive anthropogenic use of water and one of the primary agricultural practices [8]. Due to land–atmosphere interactions, irrigation has substantial effects on the local climate [9].

At present, previous research on the impact of irrigation on climate have mainly focused on near-surface temperatures [9–12], energy fluxes [13,14], water vapor [15], surface parameters [16–18], and precipitation [9]. For instance, irrigation can transform the water

and energy fluxes from the land surface to the atmosphere by enhancing soil moisture and evapotranspiration (ET). This can increase atmospheric humidity, causing additional heat stress to human bodies in some humid areas [19,20]. It has been demonstrated that irrigation has a cooling effect on the air temperature (Tem) and land surface temperature (LST) through potentially shifting sensible heat flux to latent heat flux [7,14,16,21]. At the same time, shading from the vegetation canopy reduces heat storage, which could also cool the LST [22]. On the positive side, a lower LST can help reduce heat stress on crops, which is particularly beneficial during heatwaves or in regions with high temperatures [2,23]. On the negative side, in some cases, excessively low LST can slow down crop growth, and crops may experience delayed development and maturity under consistently lower temperatures [24,25]. Moreover, a lower LST may affect the adaptability of certain crops for a region, and it may become more beneficial to cold-tolerant varieties [26]. In addition, irrigation might enhance precipitation by significantly increasing regional atmospheric water vapor content [9]; however, its cooling effect enhances the atmosphere's stability, which has a negative influence on the local precipitation [21]. In some areas, the irrigation cooling effect (ICE) has been found to alleviate and even offset the warming effect from anthropogenic greenhouse gas emissions [7,11,27–29].

Irrigation should be considered as another crucial anthropogenic climate element that should be considered in the next generation of historical climate simulations and multi-model assessments [30]. The ICE can be used as a climate regulation service [1], and disregarding its effects may lead to bias or even opposite conclusions when projecting irrigation-driven climate change. The ICE on LST can modulate the near-surface Tem through the interaction of heat flux between the land and atmosphere [10,31]. Although Tem and LST are related, their influencing factors and physical meaning are different. The Tem is mainly determined by atmospheric conditions, but LST is also greatly affected by soil moisture, surface energy fluxes, and surface properties. LST is more sensitive to surface changes caused by human activities (e.g., irrigation). It can be regarded as an excellent indicator of climate change, which provides a new perspective for us to understand the impact of irrigation on the land surface [32].

On a large regional scale, the ICE on surface temperatures has been studied mainly through climate models and observation data of meteorological stations over the past few decades [10,12,33,34]. With the development of remote sensing technology, a lot of remote sensing and reanalysis data have appeared. The MODIS LST was widely evaluated by using field observations and other remote sensing data in China and worldwide [35–37]. It overcomes the challenge of widely measuring LST over a large area and has been used to evaluate the impact of irrigation on LST around the globe [14,16]; however, the relationship between the ICE on regional LST and other irrigation effects needs further investigation. What is more, the conclusions about the influence direction of irrigation on LST and Tem are inconsistent, or the magnitudes of the ICE are greatly different in some areas with extensive irrigation [10,16,32,34,38]. This may be caused by different methods used to detect irrigation effects, and each method has its limitations. For instance, the simulation results are overly dependent on the simulation capability of the model for irrigation. As for remote sensing observations, it is difficult to eliminate the influence of other stress factors due to the difference of the distribution location and the background climate between irrigated and non-irrigated areas in a large region. This study is mainly based on multi-source remote sensing data; therefore, we have attempted to separate the irrigation effects from the effect of other factors as much as possible.

Generally speaking, the irrigation effect on LST is mainly characterized by the LST difference between irrigated and adjacent non-irrigated areas [14,38]. At the regional scale, researchers use a moving window strategy to control background differences between the comparisons. The moving window refers to a virtual rectangular or circular window that can slide or move in geographic space and is originally used to calculate statistical data within a specific range around each location in geographic space. Recently, researchers added elevation constraints to an adaptive moving window to study the irrigation effect

on LST [32,38]. To some extent, this controlled the background differences between the irrigated and non-irrigated areas used for comparison; however, directly eliminating meteorological differences or using a new index to describe ICE are promising methods. The canopy temperature depression is the difference between the canopy temperature and air temperature [39], and it is the result of the energy balance of the leaves, which are more sensitive to the changing environment [40]. It can indicate the ability of transpiration to cool the leaves [41]. Similarly, the difference between the cropland LST and the corresponding Tem (DCT = LST − Tem) can characterize the ability of ET to cool the surface. DCT links LST with Tem, making it more meaningful to study the irrigation effect, and the DCT difference between irrigated and non-irrigated areas (ΔDCT) can also be used to assess the ICE.

Based on this information, we propose an improved moving window searching strategy to detect the ICE and use the two indexes (ΔLST and ΔDCT) to evaluate the impact of irrigation on LST. With this algorithm, we determined the size of the moving window. In addition to limiting the elevation of the pixels, meteorological data were added in the moving window to control the Tem difference between the irrigated pixels and non-irrigated pixels. Based on multi-source remote sensing data of the NCP, the objectives of this study are (1) to use ΔLST and ΔDCT to comprehensively investigate the spatiotemporal patterns of the irrigation effect on the LST and compare our results with those obtained by a previous detection algorithm; (2) to determine the irrigation-induced differences of ET, the meteorological and vegetation conditions, and their spatiotemporal variability; and (3) to explore the relationships among the irrigation effects on LST, Tem, precipitation, NDVI, and ET and identify the key driving factors of the ICE.

2. Materials and Methods

2.1. Study Area

The NCP, located in the eastern part of mid-latitude Eurasia, is the heartland of modern China. It covers seven provinces or municipalities (Hebei, Shandong, Henan, Anhui, and Jiangsu provinces, Beijing and Tianjin; Figure 1). It has a warm and semi-humid continental monsoon climate with noticeable seasonal differences and abundant light and heat resources. It is an important base of grain, cotton, and oil production in China and is dominated by irrigated agriculture [42]. The primary cropping system is the winter wheat and summer maize rotation [43]. Precipitation mainly occurs in the corn growing season (June–September), and only 20–30% of it occurs in the winter wheat growing season [44].

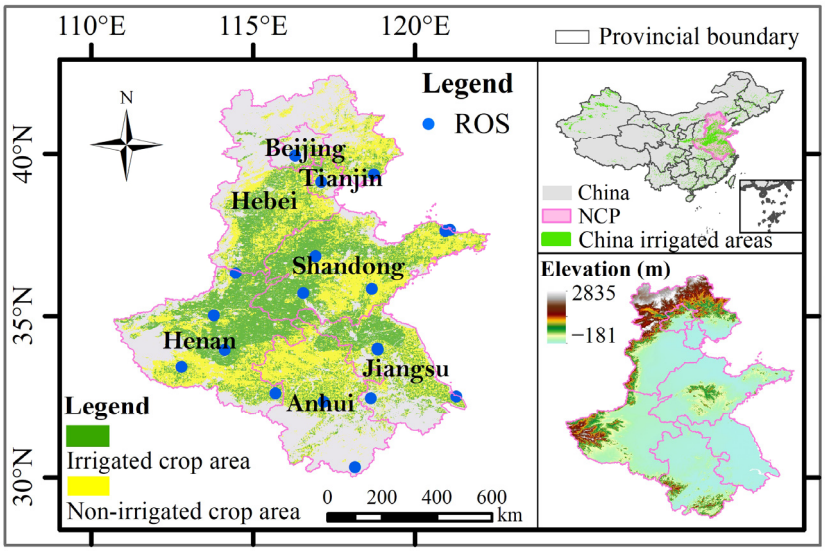

Figure 1. Location of the North China Plain (NCP) and its topographic elevation map, as well as spatial distribution of the irrigated and non-irrigated crop areas and radiation observation stations (ROS) in the NCP.

2.2. Datasets Collection

2.2.1. Meteorological Data

The 1 km resolution dataset of the monthly mean air temperature and precipitation from 2000 to 2015 used in this study was provided by Peng et al. (2019) [45], and can be obtained from the National Earth System Science Data Center, National Science and Technology Infrastructure of China (http://www.geodata.cn (accessed on 2 July 2021)). It has been verified to be reliable by the data from 496 independent meteorological observation stations. The 2000–2014 daily effective radiation dataset (Figure S1) based on 18 radiation observation sites distributed across the NCP were obtained from the Global Change Research Data Publishing and Repository (http://www.geodoi.ac.cn (accessed on 10 March 2022)) provided by Cao et al. (2018) [46].

2.2.2. Elevation Data

The 90 m Shuttle Radar Topography Mission (SRTM version 4.1) digital elevation data (Figure 1) was sourced from the Resource and Environment Science and Data Center, Chinese Academy of Science (http://www.resdc.cn (accessed on 15 May 2021)). It was used to reduce the influence of topographic relief when quantifying the cooling effect of irrigation.

2.2.3. NDVI and LST

The 2000–2015 dataset of the monthly normalized difference vegetation index (NDVI, 500 m) and land surface temperature (LST, 1 km) were the composite products of China provided by the Geospatial Data Cloud site, Computer Network Information Center, Chinese Academy of Sciences (http://www.gscloud.cn (accessed on 15 May 2021)). The NDVI dataset was derived by converting daily MOD09GA data based on Terra satellite observations to NDVI, and then aggregating the daily NDVI data into monthly maximum values. The composite LST products, including MODLT1M (started in February 2000) and MYDLT1M (started in July 2002), were derived from the MODIS version-6 LST products from the Terra satellite (MOD11A1, 1 km and 8-day) and the Aqua satellite (MYD11A1, 1 km and 8-day), respectively. The monthly MODLT1M product is ready-made. The MYDLT1M product was obtained by calculating the monthly average of the daily LST. We filtered the temperature products according to their data quality control (QC) layers to remove data with an error >1 °C. The data included the temperatures observed during daytime (local solar time ~10:30 from Terra and ~13:30 from Aqua) and nighttime (~22:30 from Terra and ~1:30 from Aqua) under a clear sky. If the LST data were available from both Terra and Aqua, we used the mean value of MODLT1M and MYDLT1M; otherwise, we used the data from the available satellite.

2.2.4. Cropland Map and ET

The MODIS 2001–2015 annual Land Cover Type product (MCD12Q1) and 2000–2015 8-day evapotranspiration (ET) product (MOD16A2) with 500 m resolution (https://ladsweb.modaps.eosdis.nasa.gov (accessed on 10 May 2021)) were used to generate the yearly dominant land cover types and monthly ET, respectively. The ET product has been proven to perform well when validated against eddy covariance flux towers over the NCP [38]. Based on the yearly IGBP classification (LC_Type1), we extracted the pixels that were constant croplands in the NCP from 2001 to 2015 as the cropland map.

2.2.5. Irrigation Map

The spatial distribution of the irrigated and non-irrigated areas in the NCP was obtained from the irrigation map provided by Meier et al. (2018) [47]. The irrigation map covers the period from 1999 to 2012 and depicts the irrigated and non-irrigated areas with a high spatial resolution (~1 km). It has been validated to reflect the actual irrigated area on global and regional scales. It has been used in research both globally and in regions

of China [14,32,38]. In this study, only the irrigated and non-irrigated pixels within the cropland map were investigated.

All of the datasets used in this study are summarized in Table 1. The preprocessing of the raster data, including mosaic, reprojection, resampling, and clipping, was completed in ArcGIS 10.2. In order to match the spatial resolution, all the spatial datasets were uniformly resampled to 1 km. The land cover data were resampled using the nearest neighbor interpolation, and the other data were resampled with a bilinear interpolation.

Table 1. The datasets used in this study. Tem = air temperature, Pre = precipitation, ERA = effective radiation.

Data Type	Product	Resolution	Period	Source
Mean Tem Pre	Peng et al. [45]	1 km, monthly	2000–2015	http://www.geodata.cn (accessed on 2 July 2021)
ERA	Cao et al. [46]	sites, daily	2000–2014	http://www.geodoi.ac.cn (accessed on 10 March 2022)
Elevation	SRTM V4.1	90 m, /	/	http://www.resdc.cn (accessed on 15 May 2021)
NDVI	MODND1M	500 m, monthly	2000–2015	
LST	MODLT1M MYDLT1M	1 km, monthly	2000–2015 2002–2015	http://www.gscloud.cn (accessed on 15 May 2021)
ET	MOD16A2	500 m, 8-day	2000–2015	https://ladsweb.modaps.eosdis.nasa.gov (accessed on 10 May 2021)
Land cover	MCD12Q1	500 m, annual	2001–2015	
Irrigation map	Meier et al. [47]	1 km, /	Spanning 1999–2012	https://doi.pangaea.de (accessed on 5 May 2021)

2.3. Method for Measuring Irrigation Effects

In this study, the ΔLST and ΔDCT were used to characterize the ICE on LST, respectively. They were defined as

$$\Delta LST = LST_{irrigated} - LST_{non\text{-}irrigated} \quad (1)$$

$$DCT = LST - Tem \quad (2)$$

$$\Delta DCT = DCT_{irrigated} - DCT_{non\text{-}irrigated} \quad (3)$$

where LST is the land surface temperature; Tem is the air temperature; and the subscripts "irrigated" and "non-irrigated" represent the irrigated pixel and adjacent non-irrigated pixel, respectively; all the units are in °C. The key element is determining how to select the irrigated and non-irrigated pixel for comparison. Based on the self-adaptive moving window searching strategy of Yang et al. (2020) [32], we adapted their "self-adaptive moving window" to a fixed-size moving window suitable for the NCP. When detecting the irrigation effect, it is necessary to constrain the influence of different background conditions in the window, such as terrain fluctuation and meteorological differences; therefore, the irrigated and non-irrigated pixels must be close enough to have a similar climate, and their elevation difference and meteorological difference are small. To satisfy the criteria above, Yang et al. limited the elevation difference (ΔE) between irrigated and non-irrigated pixels when detecting the effect of irrigation on LST. On this basis, we eliminated the influence of meteorological differences on ΔLST by restraining the average air temperature difference (ΔaveTem) between the irrigated and non-irrigated pixels in the window. In addition, we used a similar module to detect the ICE based on ΔDCT. The effects of irrigation on NDVI, ET, Tem, and precipitation were also studied using the same strategy. The searching strategy of the improved moving window algorithm is provided in Figure 2.

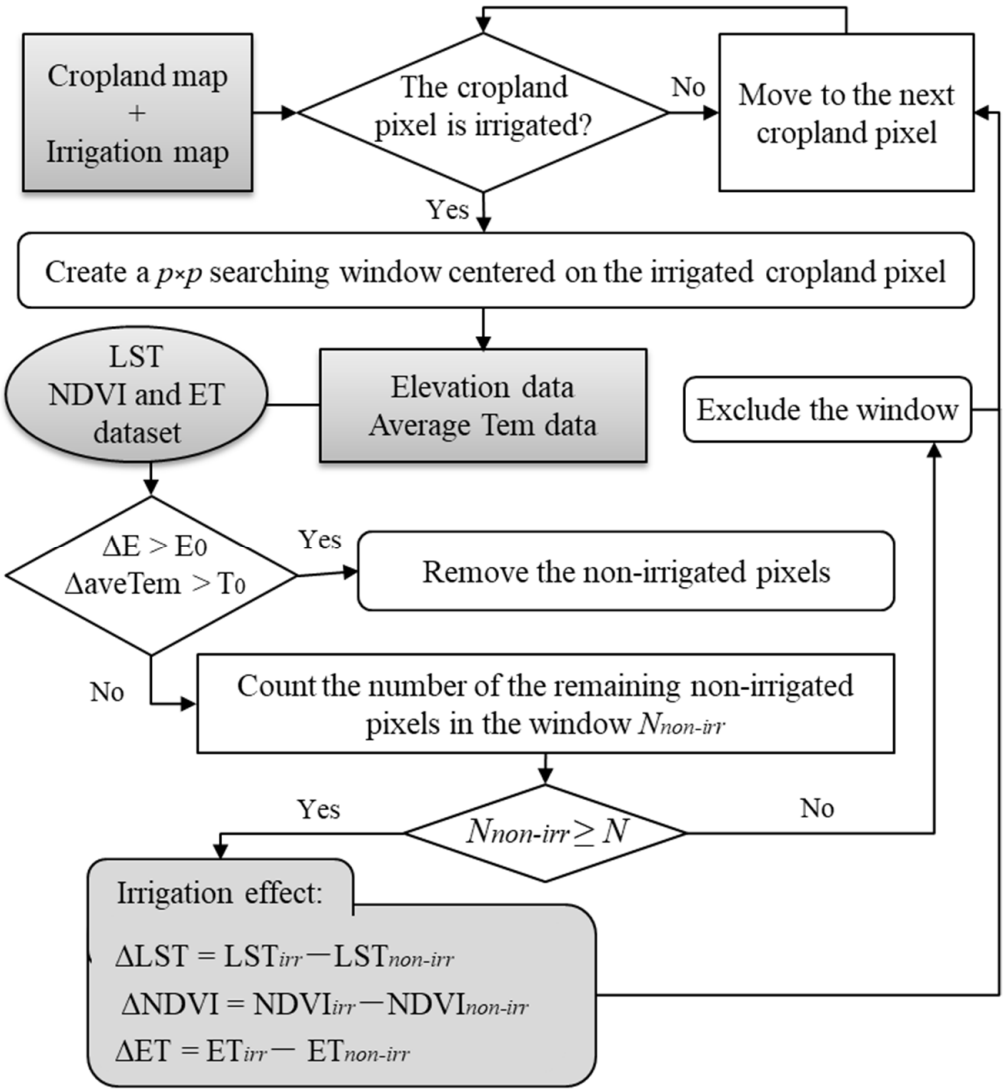

Figure 2. Algorithm for detecting the effects of irrigation on multiple indexes (LST, NDVI, ET, etc.). p = 31 pixels, E0 = 50 m, T0 = 0.3 °C, N = 15 pixels. Negative (positive) ΔLST indicate a cooling (warming) effect on LST; negative (positive) ΔNDVI and ΔET indicate that irrigation has an inhibiting (a promoting) effect on them.

We created a square window centered on an irrigated pixel and searched for non-irrigated pixels around the irrigated pixel in the window. At each window, when ΔE and ΔaveTem were greater than E0 and T0, the non-irrigated pixels were removed. The number ($N_{\text{non-irr}}$) of the remaining non-irrigated pixels was expected to be larger than the threshold value (N) to ensure the representation of the non-irrigated areas. Otherwise, this window was excluded. The default values of these parameters in this method were set as p = 31 pixels, E0 = 50 m, T0 = 0.3 °C, and N = 15 pixels. The Δ refers to Yang et al. (2020) [32]. Before deciding the other parameters, we tested their sensitivity by setting different values around the default values (Text S1). The results show that although their values had different influences on the detection of the ICE in different seasons, the ΔLSTs identified under the default parameter values were stable at an average level (Figure 3a) and have high correlations with those identified under other settings (Figure 3b). This reflects the robustness of the default parameter values in the method.

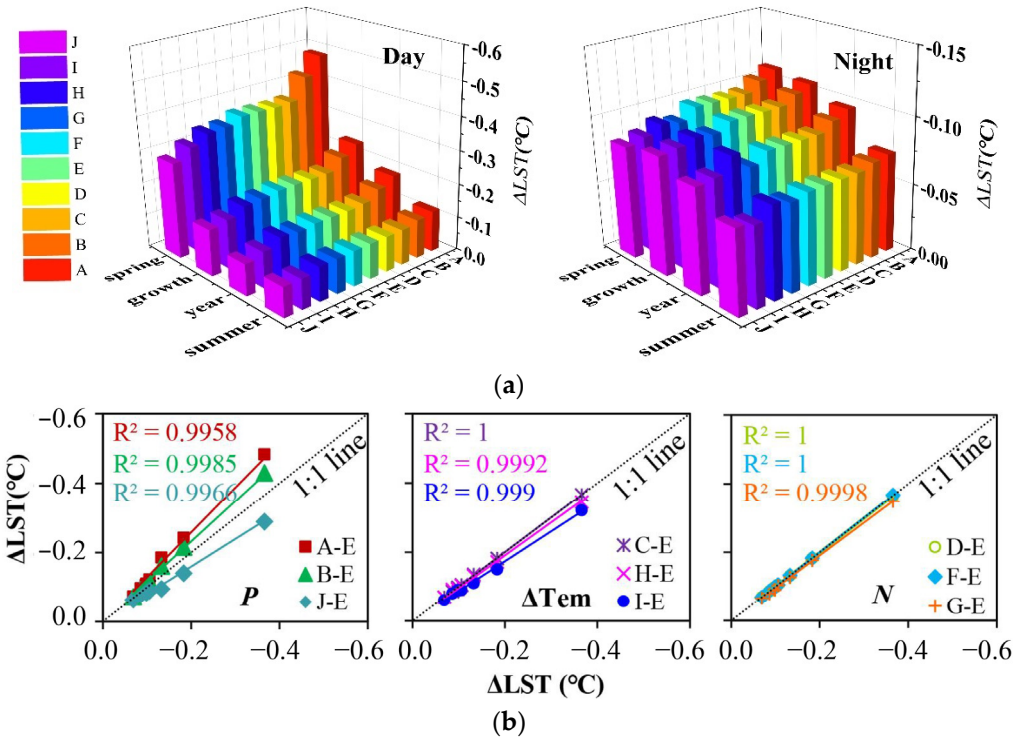

Figure 3. Sensitivity analysis of parameters *p*, ΔTem, and *N*. The default setting is E with *p* = 31, ΔTem = 0.3, and N = 15. The comparison settings fix two parameters and set different values for the other parameter; *p* is 51, 41, and 21 in A, B, and J; ΔTem is 0.2, 0.5, and 0.7 in °C, H, and I; N is 10, 20, and 5 in D, F, and G. (**a**) Comparison of the average annual daytime and nighttime ΔLSTs obtained under different settings; (**b**) correlation between the ΔLSTs of the default setting and comparison settings.

2.4. Data Analysis

In this study, IBM SPSS Statistics 26, MATLAB R2019b, Origin 2019b, and R 4.04 were used for the statistical analysis and creating the figures.

2.4.1. Linear Regression Analysis

A unary linear regression model was used to estimate the slope of the variable at the regional scale to analyze the temporal change trend of the variable. A multivariable linear regression model was used to determine the influence amplitude and direction of the other factors on the ICE. The issues of multicollinearity and autocorrelation were assessed based on the variance inflation factor (VIF) and the Durbin–Watson (DW) test. The results indicate that there were no significant multicollinearity and autocorrelation issues among the variables. In the regression model, the slope coefficient represents the change of the dependent variable as the independent variable changes by one unit, which can be used to explain the sensitivity of the dependent variable to the driving factors. A slope < 0 indicates that the dependent variable decreases as the independent variable increases. The relative importance of the variables in the multivariable linear regression model was calculated by the "relaimpo" package in R 4.04.

2.4.2. Spatial Variation Trend Test

Sen's slope has the advantages of eliminating outlier interference and avoiding missing data. It is commonly used to detect the changing trend of long time series data. In the study, Sen's slope was estimated to detect the spatial variation trends of the irrigation effects at a pixel scale from 2000 to 2015, and the Mann–Kendall test was used to test the significance of the variation trend estimated by Sen's method. The significance level is $p < 0.05$, i.e., the absolute value of the Mann–Kendall test result is greater than 1.96.

2.4.3. Correlation Analysis

The Pearson correlation can describe the degree of linear correlation between two variables. We used the "rcorr" package in R 4.04 to calculate the Pearson correlation coefficient matrixes to explore the relationship between the irrigation effects.

3. Results

3.1. Spatiotemporal Patterns of ICE Based on LST and DCT

3.1.1. Temporal Variations of ΔLST and ΔDCT

The daytime ΔLST and ΔDCT (ΔLST_d and ΔDCT_d) had the same apparent seasonal variation (Figure 4A). They showed a stronger ICE during the growing season (March–September) than the non-growing season, and the daytime ICE (ICE_d) was much higher than the nighttime ICE (ICE_n, mean value < 0.1 °C, Figure 4B(f)), especially during spring; however, the nighttime ΔLST (ΔLST_n) was generally smaller than the nighttime ΔDCT (ΔDCT_n) during the growing season (Figure 4A(b1)), which indicates that ICE_n based on LST was stronger than that based on DCT. The strongest ICE_d occurred from April to May, with an average ΔLST_d and ΔDCT_d of −0.47 °C (Figure 4A(a1)). The strongest ICE_n based on LST and DCT occurred in May and June–August, with an average ΔLST_n and ΔDCT_n of −0.13 and −0.08 °C, respectively (Figure 4A(b1)). During the growing season, the percentage of negative ΔLST_d varied from 55% to 78%, with more than 15% less than −1 °C (Figure 4A(a2)), and the average ICE_d varied from −0.06 to −0.47 °C, with an average of about −0.22 °C (Figure 4A); however, during the non-growing season, the percentage of ΔLST < −1 °C was only around 4%, and the average ICE was about −0.03 °C (Figure 4A).

During spring, the average ΔLST_d and ΔDCT_d varied from −0.15 to −0.47 °C and −0.17 to −0.47 °C, with an average of about −0.37 ± 0.79 °C and −0.36 ± 0.94 °C, respectively. During the whole year, the average annual ΔLST_d and ΔDCT_d were about −0.13 ± 0.46 °C and −0.14 ± 0.47 °C, respectively (Figure 4B(c)). At night, the ICE_n fluctuated gently throughout the year; about 70–88% of the ΔLST_n were negative, but only about 2% were less than <−1 °C (Figure 4A(b2)). The ΔLST_n and ΔDCT_n were mainly between −0.04 and −0.13 °C, with an average ICE_n ranging from −0.06 to −0.10 °C in the spring and throughout the year (Figure 4B(f)). In general, irrigation had different cooling effects with seasonal changes. From 2000 to 2015, the average ICE_d decreased insignificantly by about 0.01 °C 10 yr^{-1} in the spring (Figure 4B(a)), and increased insignificantly by about 0.03 °C 10 yr^{-1} throughout the year (Figure 4B(b)); however, the average ICE_n increased significantly by about 0.04–0.05 °C 10 yr^{-1} in both the spring- and year-scales (Figure 4B(d,e)).

3.1.2. Spatial Variations of ΔLST and ΔDCT

The spatial patterns of the average ΔLST and ΔDCT from 2000 to 2015 all showed great spatial heterogeneity in different seasons, especially during daytime in the spring (Figure 5A). For example, the range of spring ΔLST and ΔDCT was relatively large (−6.92–5.42 °C and −7.05–5.15 °C, Figure 5A(a1,f1)). The obvious ICE mainly appeared in the northern NCP (Figure 5A(a1)). From north to south, the ICE tended to weaken as the climate changed from dry and cold to humid and hot (Figure 5). In addition, it was found that at the edge of the agricultural areas, where the cropland was more fragmented, the ICE was usually much weaker, even transforming into a warming effect (Figure 5A(①–⑫)). Across the NCP, about 60% of the irrigated cropland experienced the ICE, with about 65% of the spring ΔLST_d and ΔDCT_d being negative. About 16–20% and 37–42% showed a stronger average ICE (<−0.5 °C) in the year- and spring-scale, respectively (Figure 5B). As the percentage of the stronger ICE decreased, the average ICE in different seasons decreased gradually (Figure 5). The spatial heterogeneity of ΔLST_n and ΔDCT_n was not as noticeable as ΔLST_d and ΔDCT_d, with a range of −2.00–4.83 °C (ΔLST_n) and −2.32–5.00 °C (ΔDCT_n) (Figure 5A(d2,e2)). About 52% and 40% of the irrigated areas showed that ΔLST_n and ΔDCT_n were between −0.5 and 0 °C, but less than 13% showed a

stronger ICE (Figure 5B). The average ICE_n was also almost zero over the NCP (no more than −0.1 °C, Figure 5A(a2–f2)).

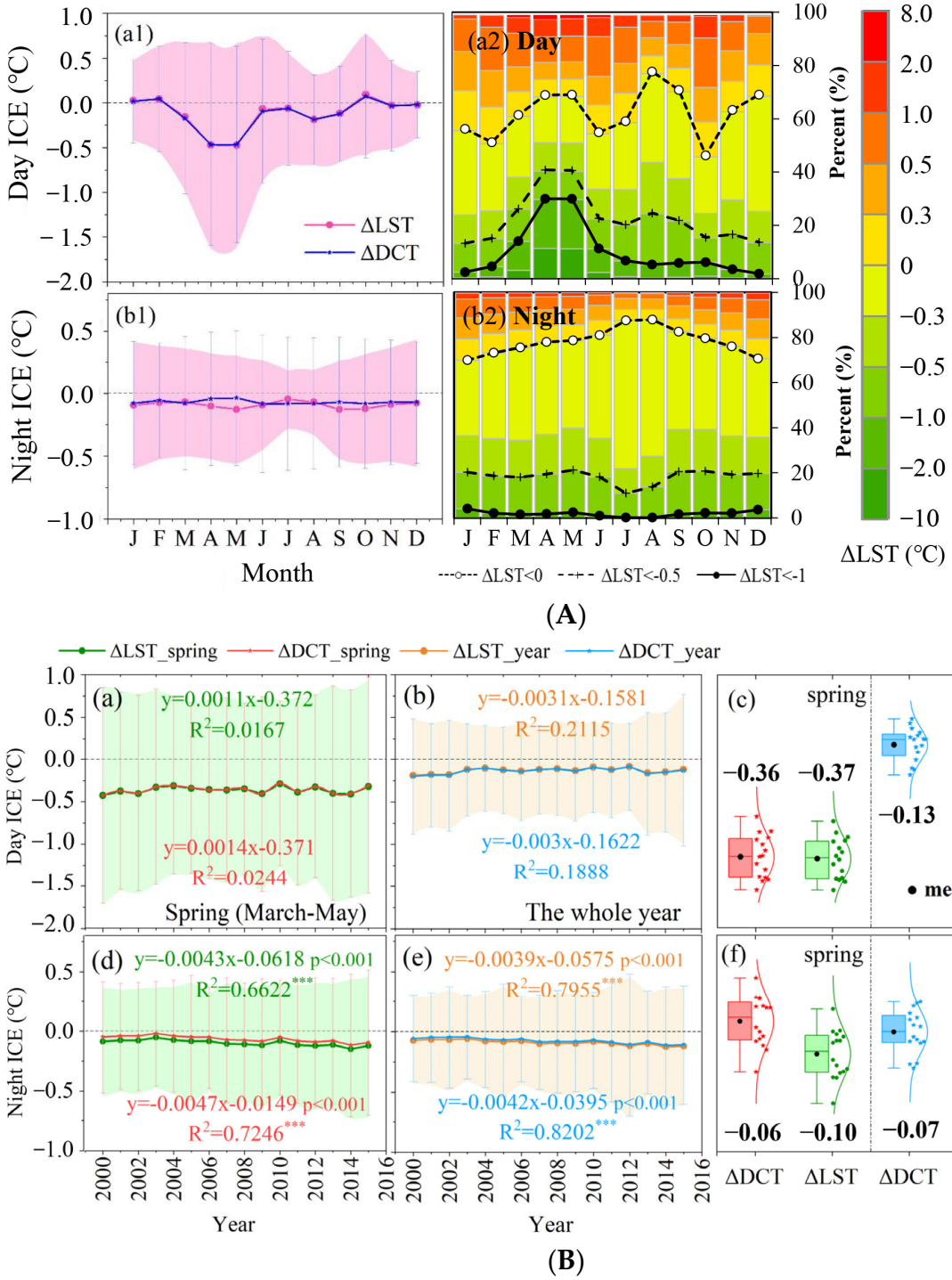

Figure 4. Temporal patterns of seasonal and annual effects of irrigation on land surface temperature (LST) and DCT (LST−air temperature). ΔLST and ΔDCT indicate the LST and DCT difference between irrigated and non-irrigated areas. Negative ΔLST and ΔDCT indicate the irrigation cooling effect (ICE). ***, $p < 0.001$. (**A**) Seasonal variations and stacked frequency distributions of the daytime (**a1**,**a2**) and nighttime (**b1**,**b2**) ICE; (**B**) annual variations of the mean and STD of the daytime (**a**–**c**) and nighttime (**d**–**f**) ICE.

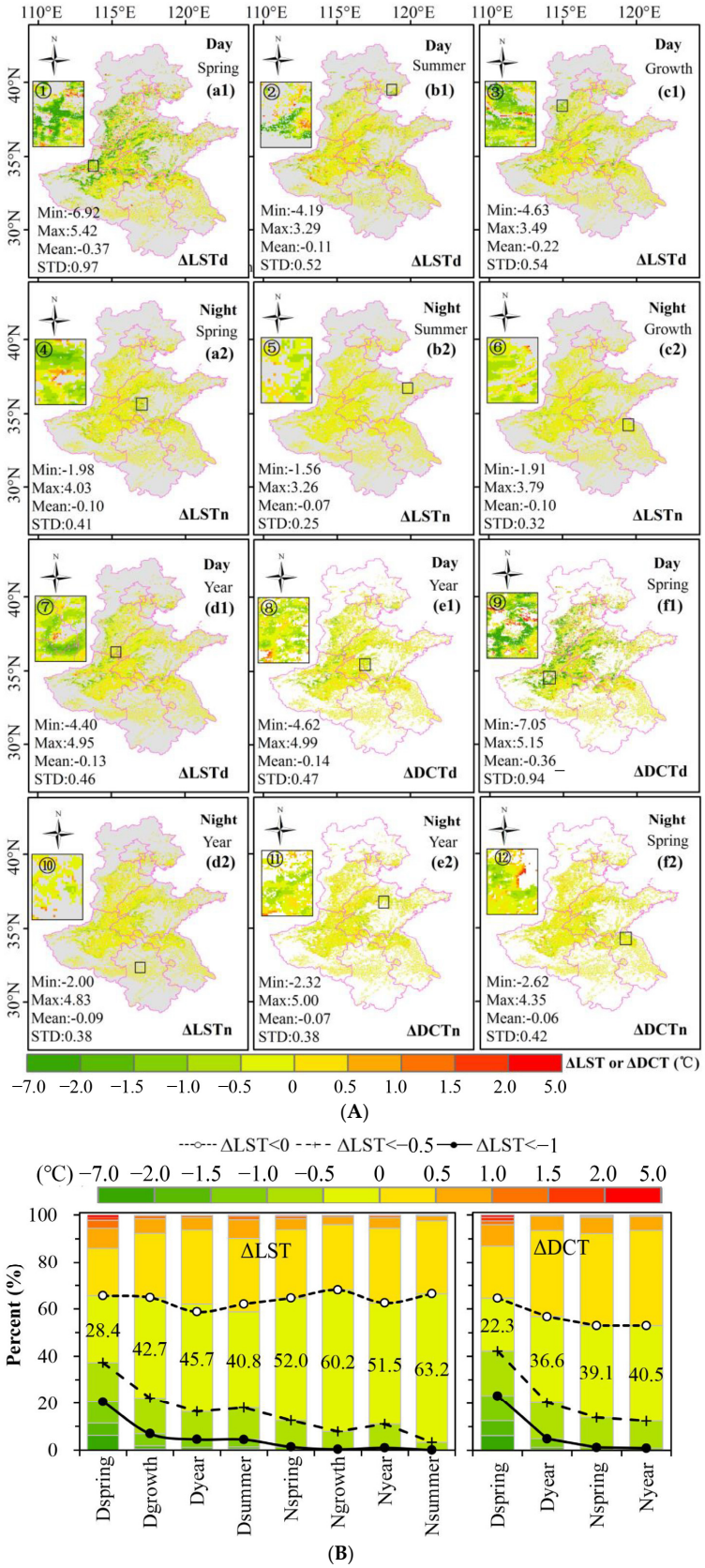

Figure 5. Spatial patterns of the average seasonal and annual effects of irrigation on land surface temperature (LST) and DCT (LST−air temperature) over the NCP cropland from 2000 to 2015 (ΔLST and ΔDCT indicate the LST and DCT differences between irrigated and non-irrigated areas). Spring, March–May; summer, June–August; growth, March–September; year, January–December. Negative

ΔLST and ΔDCT indicate the irrigation cooling effect (ICE). (**A**) Spatial patterns of the average seasonal and annual ΔLST and ΔDCT. (**a1**–**d1**) and (**a2**–**d2**) are the daytime and nighttime ΔLST during spring, summer, growing season and the whole year, respectively; (**e1**,**f1**) and (**e2**,**f2**) are the daytime and nighttime ΔDCT during spring and the whole year, respectively. The insets ①–⑫ depict the details of ΔLST and ΔDCT in different irrigation areas. ΔLST_d (ΔDCT_d) and ΔLST_n (ΔDCT_n) are the daytime ΔLST (ΔDCT) and nighttime ΔLST (ΔDCT), respectively. (**B**) Stacked frequency distributions of the annual average ΔLST and ΔDCT in different seasons. The Dspring and Nspring are the daytime and nighttime during spring, respectively, and the meaning of other labels is similar.

In the northern NCP (Henan, Hebei, Shandong, and Tianjin), the strongest average ICE_d was as high as −0.50/−0.43 °C ($\Delta LST_d/\Delta DCT_d$) during spring (Figure 6a), which was then followed by an average ICE of −0.25 °C (ΔLST_d) during the growing season (Figure 6d), −0.18/−0.17 °C ($\Delta LST_d/\Delta DCT_d$) during the whole year (Figure 6b), and −0.14 °C (ΔLST_d) during summer (Figure 6c). The most apparent ICE occurred in Henan and Hebei province, with an average $\Delta LST_d/\Delta DCT_d$ of −0.60/−0.53 °C and −0.56/−0.42 °C during spring and −0.21/−0.20 °C and −0.23/−0.18 °C during the whole year, respectively (Figure 6a,b). For Shandong and Tianjin, the average ICE_d ($\Delta LST_d/\Delta DCT_d$) was −0.50/−0.43 and −0.34/−0.35 °C during spring and −0.15/−0.13 and −0.13/−0.17 °C during the whole year, respectively (Figure 6a,b). The average ICE_n was also weak (about −0.09 °C) in different provinces (Figure 6). In Beijing, irrigation had little effect on LST, with an annual average ICE of about −0.08 °C. In the southern NCP (Anhui and Jiangsu), although the ICE was still dominant, the average magnitude of diurnal ICE was small (about −0.07 °C), varying from −0.04 to −0.11 °C in different seasons. The magnitude of the ICE_n was almost the same as that of ICE_d, or even higher (Figure 6a,b).

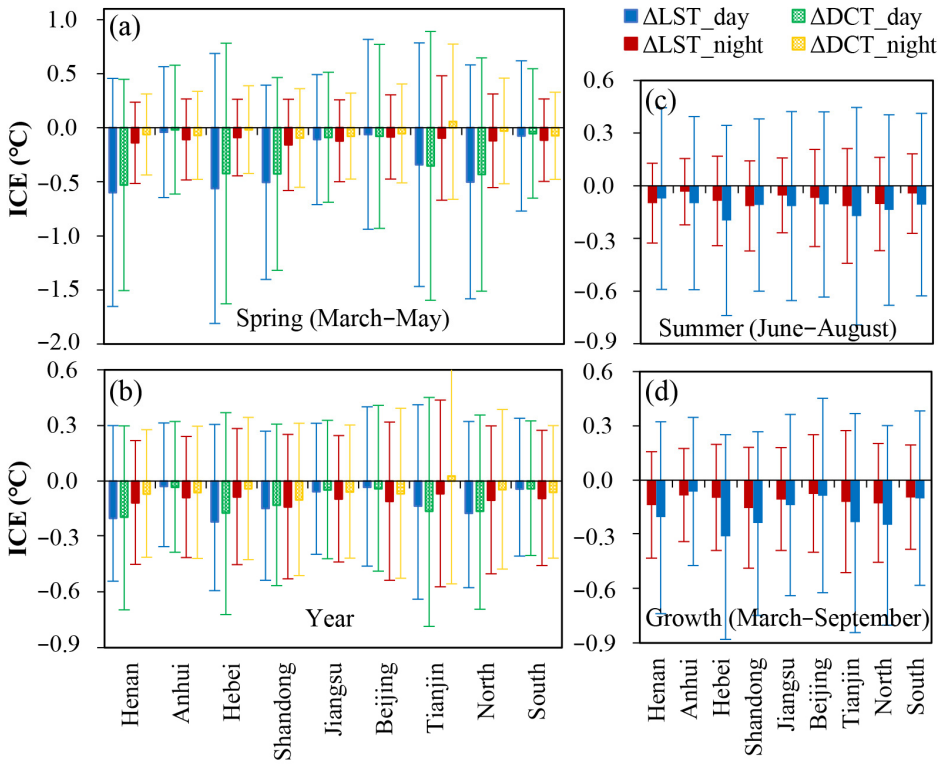

Figure 6. The annual average ICEs (ΔLST and ΔDCT ± SD) in different administrative districts of the NCP during spring (**a**), the whole year (**b**), summer (**c**) and growing season (**d**). The North and South represent the northern and southern parts of the NCP, respectively. ΔLST and ΔDCT indicate the land surface temperature (LST) and DCT (LST−air temperature) differences between irrigated and non-irrigated areas.

3.2. Comparison of the ICEs Quantified by Different Methods

The spatiotemporal pattern of the LST difference (ΔLST_{dem}, Figure S2) between the irrigated and non-irrigated areas calculated by the previous algorithm [32] was similar to that calculated by our improved algorithm (ΔLST, Figure 5A) in different seasons; however, their magnitudes at the pixel scale were very different in some areas, with over 50% and 70% of the ΔLST_{dem} greater than ΔLST during nighttime and daytime, respectively (Figure 7). The average difference varied between 0.005 °C and 0.034 °C, which accounted for 4.55–18.89% of the average ICE quantified by ΔLST in the different seasons across the NCP (Figure 7 and Tables S1 and S2). The difference was more evident (>0.1 °C) in areas with large topographic relief, especially in spring (Figure 7(1–4)). Although the average ΔLST_{dem} of Tianjin was lower than the average ΔLST, that of other provinces was generally higher (Table S1). The average differences mainly occurred during spring, which accounted for 10.47–20.43% and 17.13–17.29% of the ΔLST in the northern and southern NCP, respectively (Figure 7 and Table S2). Throughout the year, it was as high as 12.0–21.59% in the northern NCP, but was also found to be negligible during daytime in the southern NCP (only 0.60%, Table S2). The results above indicate that, except for Tianjin, a coastal city that is greatly affected by oceanic climate, the ICE measured by ΔLST_{dem} was generally lower than that measured by ΔLST; therefore, it is necessary to add a meteorological restriction to the algorithm.

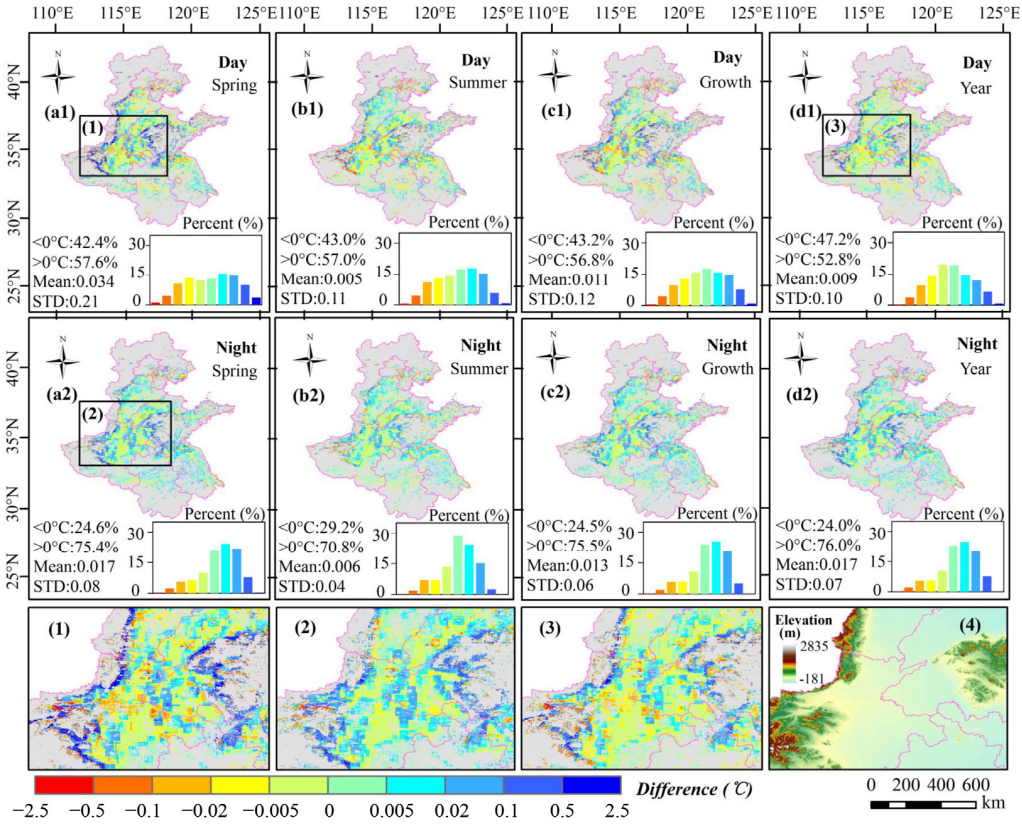

Figure 7. The differences between ΔLST_{dem} and ΔLST in the different seasons over the NCP cropland; (**a1**–**d1**) and (**a2**–**d2**) are the daytime and nighttime differences between ΔLST_{dem} and ΔLST during spring, summer, growing season and the whole year, respectively; (**1**)–(**3**) show the details within the box in the subfigures (**a1**,**a2**,**d1**); and (**4**) shows the elevation within the box. ΔLST_{dem} was calculated by the previous algorithm (Yang et al. [32]), which does not directly control the meteorological difference between irrigated and non-irrigated pixels in the moving window; ΔLST was the land surface temperature (LST) differences calculated in this study. Difference = ΔLST_{dem} − ΔLST, °C.

The average ΔLSTs were generally lower than the ΔDCTs (i.e., the ICE quantified by ΔDCT was weaker than that quantified by ΔLST) at different time scales across the NCP (Table S3). The nighttime differences (ΔICE) were relatively large, with a range and MAPE of −0.016–−0.032 °C and 17.5–33.07%, respectively; however, the daytime ΔICE were almost negligible, with a range of −0.004–0.004 °C (MAPE < 4%, Table S3). The same pattern appeared in the south and north of the NCP and in different administrative districts (Table S4). In general, the diurnal ΔICE was acceptable at different time scales, with a range and MAPE of −0.006–−0.018 °C and 5.19–7.73%, respectively (Table S3). The ΔDCT can capture the irrigation effect in a more detailed way at the spatial pixel scale, with a broader range of −2.60–4.35 °C in spring and −2.32–5.00 °C throughout the year, while that of the corresponding ΔLST was −1.98–4.03 °C and −2.0–4.83 °C, respectively (Figure 5A).

3.3. Spatiotemporal Patterns of Irrigation Effects on ET, Precipitation, Tem, and NDVI

3.3.1. Temporal Patterns of Irrigation Effects on ET, Precipitation, Tem, and NDVI

Irrigation had an inhibiting effect on Tem and precipitation (ΔTem and ΔPre were generally negative) and a promoting effect on ET and NDVI (ΔET and ΔNDVI were generally positive) (Figure 8A). The effects had a similar seasonal variation to the ICE (i.e., stronger in the growing season, especially in spring), and their variation trends were synchronous in spring (Figures 4 and 8A). During the growing season, the ΔPre showed a bimodal curve and ranged from −0.069 mm (March) to −0.392 mm (July), with the other peak appearing in April (about −0.154 mm) with an average of about −0.153 mm month^{-1} (Figure 8A). The ΔTem, ΔET, and ΔNDVI showed a unimodal pattern, peaking in April–May. Their ranges were 0.012 °C (June)–−0.039 °C (May), 0.003 mm (September)–0.106 mm (May), and 0.005 (June)–0.035 (April), with an average of about −0.005 °C month^{-1}, 0.035 mm month^{-1}, and 0.021 month^{-1}, respectively. During the non-growing season, the magnitude of ΔPre, Δtem, ΔET, and ΔNDVI was negligible, averaging about −0.078 mm month^{-1}, 0 °C month^{-1}, 0 mm month^{-1}, and 0.015 month^{-1}, respectively.

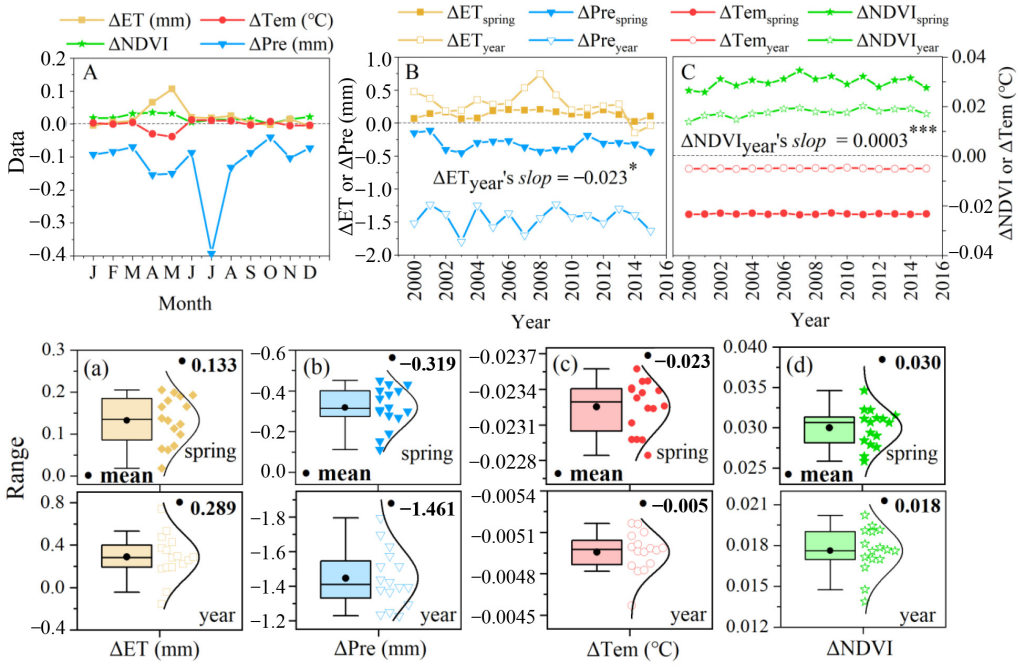

Figure 8. Seasonal (**A**) and annual (**B**,**C**) variations of the average ΔET, ΔPre, ΔTem, and ΔNDVI over the NCP cropland from 2000 to 2015; (**a**–**d**) are box plots showing the dispersion of spring and annual ΔET, ΔPre, ΔTem and ΔNDVI during 2000–2015. ΔET, ΔPre, ΔTem, and ΔNDVI are the difference of ET, precipitation, air temperature, and NDVI between irrigated and adjacent non-irrigated areas. Negative numbers indicate that irrigation had an inhibiting effect on the index. *, $p < 0.05$; ***, $p < 0.001$.

From 2000 to 2015, the spring and annual ΔPre varied from −0.112 to −0.451 mm and −1.230 to −1.797 mm, with a mean value of about −0.319 and −1.461 mm (Figure 8B,b). The spring and annual average ΔTem varied around the mean values, about −0.023 and −0.005 °C, respectively (Figure 8C,c). The variation range of ΔET and average ΔNDVI during the spring were 0.012–0.206 mm and 0.026–0.035, averaging about 0.133 mm and 0.03; and those throughout the year were −0.151–0.744 mm and 0.014–0.020, averaging 0.289 mm and 0.018, respectively (Figure 8). Statistically, the annual ΔET and annual average ΔNDVI respectively showed a significant negative (slop = −0.23 mm 10 yr^{-1}, $p < 0.05$) and positive (slop = 0.003 10 yr^{-1}, $p < 0.001$) trend during the 16 years. This indicates that the effects of irrigation on ET and NDVI enhanced over time.

3.3.2. Spatial Patterns of Irrigation Effect on ET, Precipitation, Tem, and NDVI

The effects of irrigation on ET, precipitation, Tem, and NDVI had similar spatial heterogeneity as the ICE across the NCP, with some pixels experiencing an inhibiting effect (negative) and some experiencing a promoting effect (positive) (Figure 9A). From the north to the south of the NCP, the average ΔET, ΔTem, and ΔNDVI decreased, while the Δpre increased (Figure 9B). Spatially, about 61% and 55% of the irrigated cropland showed negative Δpre and Δtem (Figure 9A(b,c)), and more than 51% and 70% showed positive ΔET and ΔNDVI, respectively (Figure 9A(a,d)). Throughout the year, the promoting effects on ET and NDVI were mainly 2–20 mm and 0–0.05 (about 30% and 55%), and the inhibiting effects on precipitation and Tem were mainly −2–12 mm and 0–−0.1 °C (about 41% and 48%), respectively (Figure 9A(a1,b1)). In the northern NCP, irrigation also generally inhibited precipitation and Tem, and promoted ET and NDVI, with a ΔPre, ΔTem, ΔET, and ΔNDVI of −1.229 mm yr^{-1}, −0.044 °C $month^{-1}$ (in spring), 0.316 mm yr^{-1}, and 0.033 (in spring), respectively (Figure 9B); however, in the south, the irrigation effects on Tem and ET transformed into slight inhibition (ΔTem = 0.002 °C $month^{-1}$) and promotion (ΔET = −0.056 mm yr^{-1}), respectively. The promoting effect on NDVI was weakened (ΔNDVI = 0.008 $month^{-1}$), which was only 40.0% of that in the north; however, the inhibiting effect on annual precipitation was about −1.879 mm, up to 152.9% of that in the north. It is noteworthy that the effects of irrigation on ET, precipitation, and Tem in Beijing were contrary to the results above, i.e., it promoted precipitation and Tem, and inhibited ET (ΔET = −2.454 mm yr^{-1}). This may be one of the reasons why the ICE was weak in Beijing. Excluding Beijing, the most obvious irrigation effects on ET, precipitation, Tem, and NDVI occurred in Henan (0.632 mm), Jiangsu (−2.779 mm), Tianjin (−0.077 °C), and Shandong (0.039), respectively (Figure 9B).

3.4. Spatial-Trend Slopes of Irrigation Effects

Since the irrigation effects mainly occurred in spring, the Theil–Sen median slope analysis and Mann–Kendall test of the irrigation effect in spring were performed pixel by pixel from 2000 to 2015 (Figure 10). The results show that the trend slopes of the irrigation effects were spatially heterogeneous, as well. The trend slopes of some ΔLST_d were −0.1–−0.65 °C yr^{-1}, and others were 0–0.1 °C yr^{-1}. More than half of the NCP cropland (about 52%, 60%, 51%, and 53%) showed a mean trend of −0.05 °C yr^{-1}, −0.02 °C yr^{-1}, 1.20 mm 10 yr^{-1}, and 0.03 10 yr^{-1} for ICE_d (ΔLST_d and ΔDCT_d), ICE_n (ΔLST_n and ΔDCT_n), ΔET, and ΔNDVI, respectively (Figure 10(a1–e1,h1)). Among them, about 15%, 14%, 5%, and 14% were significant, with a mean trend of about −0.10 °C yr^{-1}, −0.04 °C yr^{-1}, 2.90 mm 10 yr^{-1}, and 0.06 10 yr^{-1}, respectively (Figure 10(a2–e2,h2)). This means that the irrigation cooling effect on LST and promotion effect on ET and NDVI were strengthened. Meanwhile, the rest of ICE_d, ICE_n, ΔET, and ΔNDVI showed the opposite trends of about the same rate, of which about 14%, 8%, 5%, and 18% were significant trends (Figure 10a–e,h). In terms of the climate factors, although the positive (negative) trends of ΔPre and ΔTem occupied approximately 66% (34%) and 51% (49%), the magnitude of the trends was small, averaging about 0.28 (−0.16) mm 10 yr^{-1} and 0.006 (0.006) °C 10 yr^{-1}, respectively (Figure 10(f1,g1)). The significant positive (negative) trends of them only occupied 1.30% (0.50%) and 3.01%

(3.01%), with a mean trend of 0.66 (−0.39) mm 10 yr^{-1} and 0.015 (−0.016) °C 10 yr^{-1} (Figure 10(f2,g2)). This significant trend was mainly distributed in western Shandong and the adjacent eastern Henan (Figure 10), where the irrigated areas are concentrated and flat.

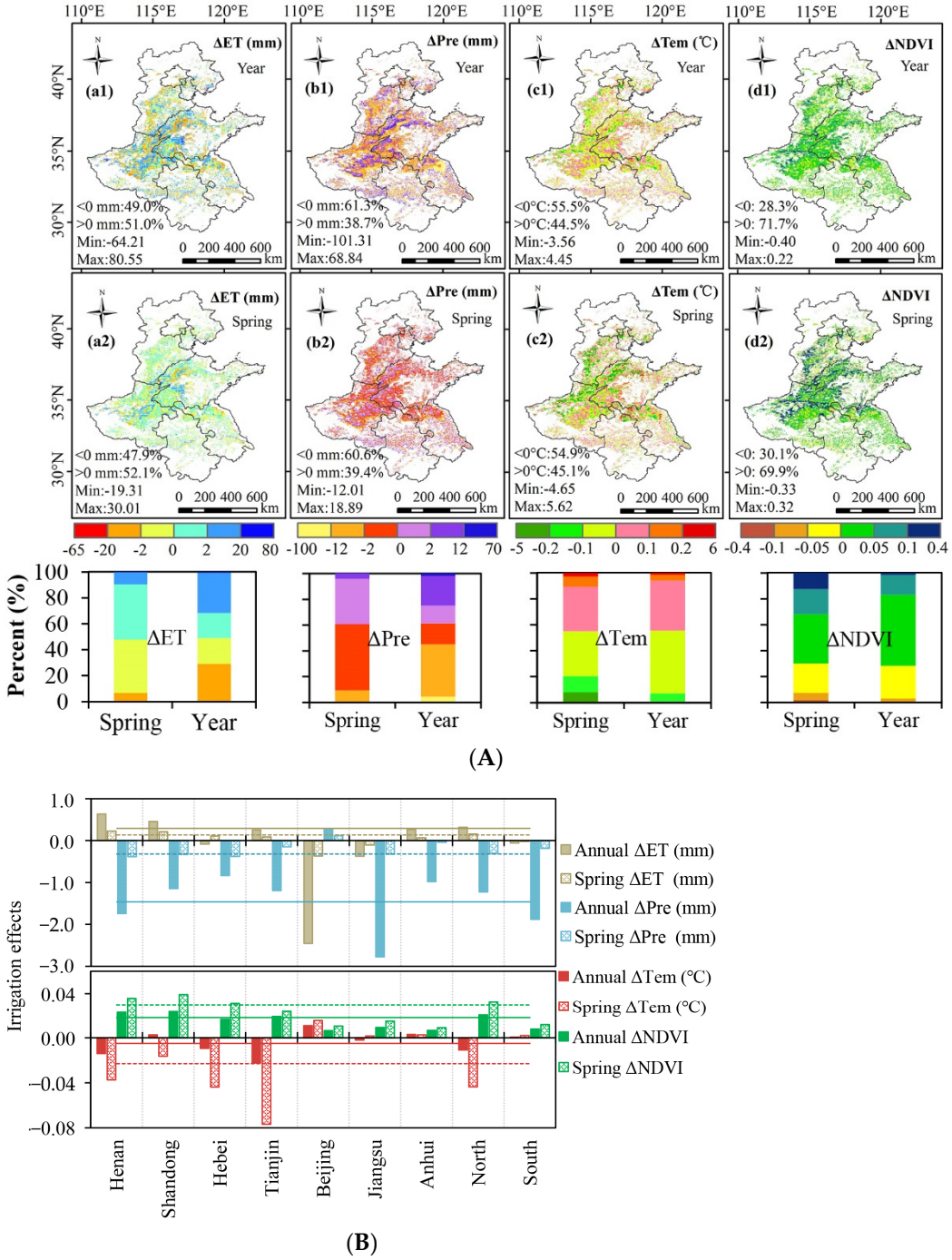

Figure 9. Spatial patterns of irrigation effects on precipitation, Tem, NDVI and ET (i.e., ΔET, ΔPre, ΔTem and ΔNDVI) during 2000–2015. (**A**) Spatial patterns and stacked frequency distributions of the annual (**a1**–**d1**) and spring (**a2**–**d2**) average ΔET, ΔPre, ΔTem and ΔNDVI; ΔET, ΔPre, ΔTem and ΔNDVI are the difference of ET, precipitation, air temperature and NDVI between irrigated and adjacent non-irrigated areas; (**B**) the irrigation effects on precipitation, Tem, NDVI and ET in different administrative districts throughout the year and spring. The North and South represent the northern and southern parts of the NCP. The colored dotted and solid lines are the mean values of the indexes across the NCP.

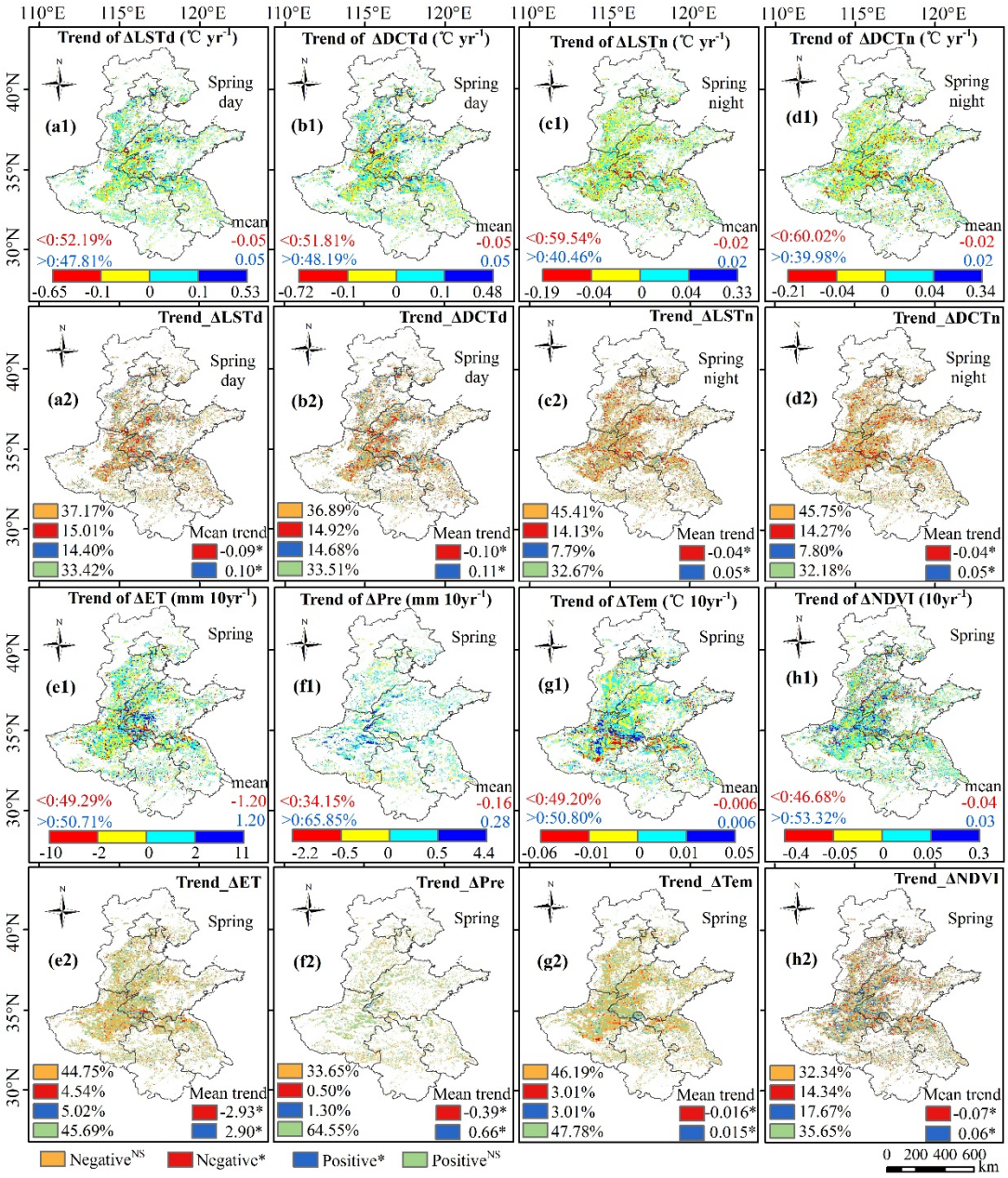

Figure 10. The distributions of spatial-trend slopes of spring ΔLST, ΔDCT, ΔET, ΔPre, ΔTem and ΔNDVI over the NCP cropland from 2000 to 2015. (**a1–h1**), the spatial-trend slopes of spring ΔLST_d, ΔDCT_d, ΔLST_n, ΔDCT_n, ΔET, ΔPre, ΔTem and ΔNDVI, respectively; (**a2–h2**), the frequency distributions of the positive and negative slopes of ΔLST_d, ΔDCT_d, ΔLST_n, ΔDCT_n, ΔET, ΔPre, ΔTem and ΔNDVI, respectively. "Δ" means the difference between irrigated and adjacent non-irrigated areas. LST_d and LST_n, daytime and nighttime land surface temperature (LST); DCT = LST−air temperature; Pre, precipitation; Tem, air temperature. The trend slopes were measured by the Theil–Sen median method coupled with the Mann–Kendall test. Significant trend is indicated as * ($p < 0.05$); non-significant trend is indicated as ^{NS}.

3.5. Factors Underlying ICE Variation

3.5.1. Relationships among NDVI, ET, Climate Factors, and ICE

The relationships between the crop factor (e.g., ΔNDVI), climate factors (e.g., ΔTem, ΔPre, and ERA), water consumption (e.g., ΔET), and ICE (e.g., ΔLST and ΔDCT) were investigated using a correlation matrix and network at a monthly scale (Figure 11). The results show that there were complex interactions among them. For example, there were

negative correlations between ΔTem, ΔLST_d, ΔDCT_d, ΔLST_n and ERA, ΔNDVI, ΔDCT_n, and ΔET, with a correlation coefficient (r) between −0.01 and −0.95. ΔTem, ΔLST_d, ΔDCT_d, and ΔLST_n were positively correlated with each other ($0.27 \leq r \leq 1$), as were ERA, ΔNDVI, ΔDCT_n, and ΔET ($0.29 \leq r \leq 0.77$) (Figure 11a). ΔPre was positively correlated with ΔLST_d, ΔDCT_d, ΔDCT_n, and ERA ($0.02 \leq r \leq 0.47$), but negatively correlated with ΔLST_n, ΔET, ΔNDVI, and ΔTem ($-0.01 \leq r \leq -0.48$). The relationships between the daytime ICE (ΔLST_d and ΔDCT_d), nighttime ICE (ΔDCT_n), ΔTem, ΔNDVI, and ΔET were significant (mostly $p < 0.01$). From the correlation network (Figure 11b), we can see that ΔNDVI and ΔET were strong negative predictors for the daytime ICE, with an r of about −0.73 ($p < 0.01$) and −0.90 ($p < 0.001$) but were strong positive predictors for ΔDCT_n (r = 0.71 and 0.77, $p < 0.01$), respectively. On the contrary, ΔTem was a strong positive and negative predictor for the daytime and nighttime ICE (r = 0.80, $p < 0.01$, and r = −0.95, $p < 0.001$), respectively. Although ΔLST_n, ΔPre, and ERA were insignificantly correlated with other indicators, they were moderately correlated with each other. In addition, ΔLST_n was moderately correlated with ΔDCT_n and ΔTem, and ERA was also moderately correlated with ΔDCT_n, ΔTem, and ΔNDVI, respectively.

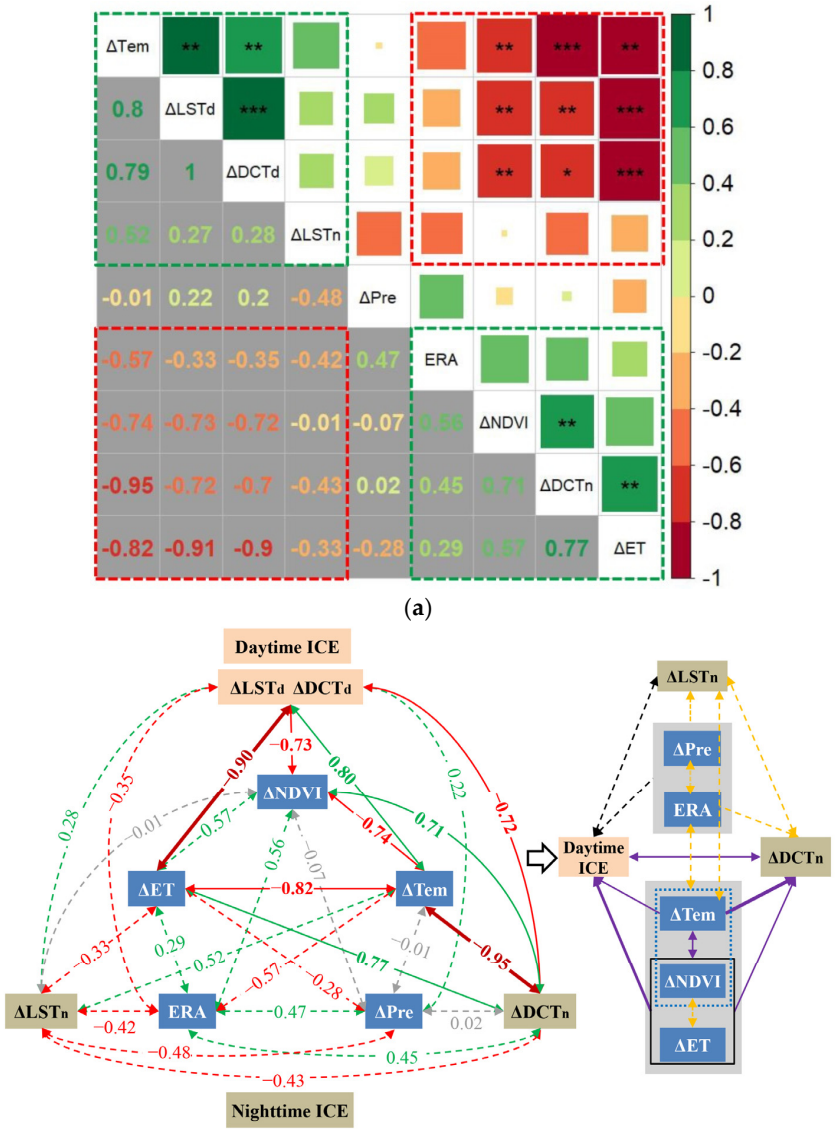

Figure 11. Correlation analysis for examining the driving factors underlying the ICE variation over the NCP cropland. ERA: effective radiation. "Δ" represents the difference of these indicators between

irrigated and adjacent non-irrigated areas over the NCP cropland. (**a**) Color-coded correlation coefficient (Pearson's r) matrix indicating the interactions of ΔNDVI, ΔET, ΔTem, ΔPre, ERA, and ICE (e.g., ΔLST and ΔDCT) over NCP cropland; *, $p < 0.05$; **, $p < 0.01$; ***, $p < 0.001$. (**b**) path diagram of correlation network exploring the intrinsic factors driving the ICE. The red, green, and gray arrows indicate negative, positive, and unrelated ($|r| < 0.1$) relationships, respectively. The solid arrows represent a significant relationship (thick, $p < 0.001$; thin, $p < 0.05$); the dotted arrows represent an insignificant relationship ($p > 0.05$). Numbers adjacent to each arrow are the correlation coefficients. The purple, yellow, and black arrows represent strong ($|r| > 0.7$), medium ($0.4 < |r| < 0.7$), and weak ($|r| < 0.4$) correlations, respectively.

3.5.2. Quantifying the Impact of NDVI, ET, and Climate Factors on ICE

At the regional scale, we quantified the impact of ΔNDVI, ΔET, ΔPre, Δtem, and ERA on ICE, as well as their total contribution and relative importance to explain the ICE variation by multiple regression and variance decomposition analyses (Figure 12). The results show that 92.4%, 74.6%, 89%, and 90.2% variation of ΔDCT_n, ΔLST_n, ΔDCT_d, and ΔLST_d, respectively, could be significantly explained by other variables in the regression model. ΔET was the most important factor to explain ΔLST_d and ΔDCT_d, accounting for 43.8% and 45.4% of R^2, followed by ΔTem (25.9% and 25%), ΔNDVI (22.8% and 22.1%), ERA (4.5% and 4.6%), and Δpre (3% and 2.8%). For ΔDCT_n and ΔLST_n, Δtem was the most important factor to explain them, accounting for 49.3% and 33.3% of R^2, followed by ET (24%), NDVI (18%), ERA (7.3%), Pre (1.4%) and Pre (23.8%), NDVI (21.1%), ET (11.1%), and ERA (10.6%), respectively. ΔLST_d, ΔDCT_d, ΔLST_n, and ΔDCT_n all showed negative sensitivity to ΔET. When ΔET increased by 1 mm, these measurements decreased by 4.458 ($p < 0.01$), 4.672 ($p < 0.01$), 0.015, and 0.018 °C, respectively. That is, the ICE on LST enhanced with the increase in the irrigation-promoting effect on ET. In addition, ΔLST_d and ΔDCT_d showed negative sensitivity to ΔNDVI, ΔTem, and ΔPre, and positive sensitivity to ERA. Both ΔLST_n and ΔDCT_n showed positive and negative sensitivity to ΔNDVI and ERA, respectively. ΔLST_n showed positive and negative sensitivity to ΔTem and ΔPre respectively, while ΔDCT_n showed the opposite. Precisely speaking, for every unit increased in the irrigation promoting effect on NDVI, ICE_d enhanced by 7.453 (ΔLST_d, $p < 0.05$) and 7.173 (ΔDCT_d, $p < 0.05$) °C, but ICE_n weakened by 1.945 (ΔLST_n, $p < 0.05$) and 0.198 (ΔDCT_n) °C, and even turned into warming effect. For every unit of ΔTem and ΔPre increased, ΔLST_d (ΔDCT_d) decreased by 1.066 (1.935) and 0.179 (0.213) °C (i.e., ICE_d enhanced), and ΔLST_n (ΔDCT_n) changed by 1.643 (−1.025) °C and −0.107 (0.023) °C, respectively. For every 100 MJ m^{-2} increased in ERA, ICE_d weakened by about 0.1 °C, but ICE_n enhanced by about 0.01–0.02 °C.

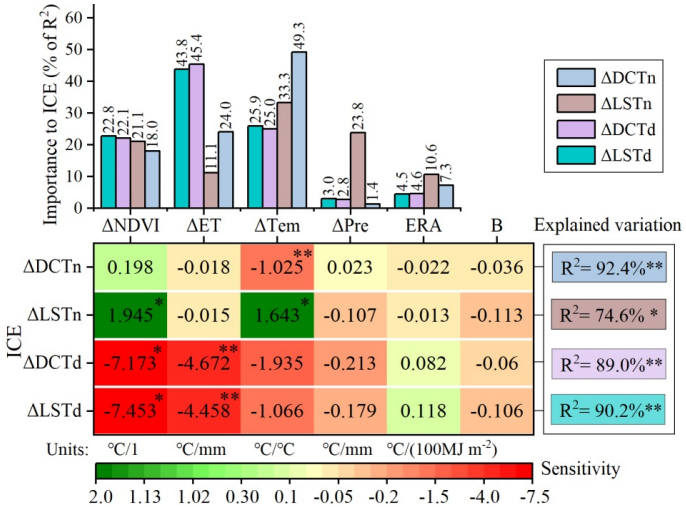

Figure 12. Contributions of other irrigation effects on crop growth, ET and climate (i.e., ΔNDVI, ΔET, ΔPre and ΔTem) and effective radiation (ERA) to ICE based on multiple linear regression model. The

heat map shows the sensitivity of ICE to these factors; the R^2 in the left block diagram shows their total contribution to explaining ICE variation; and the bar chart above shows the relative importance of each variable, which was calculated via variance decomposition analysis. *, $p < 0.05$; **, $p < 0.01$.

4. Discussion

At the regional scale, due to the different geographical locations between the irrigated areas and non-irrigated areas, the meteorological conditions are different, and the differences could also influence the LST (Figures S3 and S4). Researchers have proposed a self-adaptive moving window method to try to eliminate the influence by controlling the window size [16,48], and Yang et al. further eliminated the influence by limiting the elevation of the pixels in the window [14,32], which, when applied to a cropland irrigation map, can successfully extract the ICE. Most studies, however, have mainly used ΔTem or ΔLST to characterize the ICE, and the effect of different Tem on LST was not eliminated directly [10,11,14,16,49]. In this study, in addition to controlling the window size and pixel elevation, we added Tem to the moving window algorithm to further eliminate the effect of the meteorological difference directly. The method can be applied to other regions, especially in areas with large topographic relief and meteorological variation. Based on the improved method and satellite observations, we used ΔLST to quantify the ICE on LST and used ΔNDVI and ΔET to evaluate the effect of irrigation on NDVI and ET. In addition, based on the moving window method, we also quantified the irrigation effect on Tem and precipitation and used a new index ΔDCT (DCT = LST − Tem) connecting LST and Tem to quantify the ICE. In addition, we compared the differences between the ICEs on LST quantified by different indexes and methods and explored the impact of other irrigation effects on ICE across the NCP's cropland.

Chen and Dirmeyer (2019) and Yang et al. (2020) performed sensitivity tests for the previous moving window algorithm at different scales, and they reported ΔLST was not significantly affected by their choice of parameters in the moving window [16,32]. In this study, the sensitivity of the window size, the threshold of the Tem difference, and the number of remaining non-irrigated pixels were also tested before the experiment. The results show that although the choice of parameters had some effect on ΔLST, the default values we determined were robust in the NCP (Figure 3). Overall, the identified patterns of ΔLST were not significantly affected by the choice of parameters, reflecting the robustness of our findings. The Tem in the irrigated area was higher than that in the non-irrigated area (Figures S3 and S4), which could increase the LST of the irrigated area and mask the ICE to a certain extent; therefore, the ICE based on ΔLST assessed by the previous algorithm was generally weaker than that assessed by our proposed algorithm, especially in areas with large topographic relief (Figure 7), but it was stronger in a coastal city (e.g., Tianjin, Table S2). This may be because the climate changes greatly in the area with large relief, and the coastal area is obviously affected by the marine climate. The ICEs assessed based on ΔLST and ΔDCT were essentially the same, with the difference mainly occurring at night (Figures 4–6); however, due to the weak ICE on night LST, the intraday difference between ΔLST and ΔDCT can be ignored (Table S3). It is therefore necessary to control the Tem difference between the irrigated pixel and the non-irrigated pixel in the moving window, and ΔDCT had an excellent performance to assess the ICE.

Like many experimental results [9,14,33,38], our results also clearly support that irrigation induces a cooling effect on LST with spatial and temporal heterogeneity (Figure 4). This is supported by higher soil moisture, higher ET, and contrasting vegetation conditions over the irrigated area [16]. For instance, the ICE across China in the growing season, daytime, and arid region was stronger than that in the non-growing season, night, and humid area [32]. The results of our study over the NCP also show the same spatiotemporal pattern, but the magnitude of the ICE varied greatly, with the daytime ICE reaching 0.37 °C across the NCP and 0.50 °C in the northern NCP during spring. At present, there are two main reasons for the widely observed ICE. One is that irrigation increases soil moisture and promotes crop growth, which can enhance ET. As a result, more sensible heat fluxes are redistributed to latent heat fluxes, which directly cools the LST [14,50,51]. The other

is that irrigation can increase the atmospheric water vapor, which will lead to an increase in the cloud cover in the irrigated areas. This reduces the total downwelling radiation and indirectly cools the LST [14,30]. Yang et al. (2020) further believed that the net impact of irrigation on LST resulted from the competition between the potential warming effect induced by the lower albedo and the cooling effect created by the higher ET [14]. Moreover, other human agricultural activities (e.g., fertilization, cropping system, and agricultural development) may also have a specific impact on the ICE. For example, the ICE of a paddy was positively associated with the irrigation rate and negatively associated with the water depth [52].

In the study, the widely observed ICE over NCP can be reasonably explained by the mechanisms highlighted above. The combined effect of these mechanisms results in the spatiotemporal variation of the impact of irrigation on LST. For instance, the ICE during the growing season, especially during spring, was generally more extensive than that during the non-growing season (Figures 4 and 5). This is because irrigation occurs during the growing season, especially in spring, with less rainfall and the enormous water consumption of winter wheat [44]. During this period, irrigation promotes crop growth (higher NDVI) and ET (Figure 8), which can lead to more surface net radiation converted into latent heat fluxes, resulting in an extensive cooling effect [51]. In addition, irrigation also cools the Tem most obviously during this period (Figure 8). The ICE during the daytime is usually stronger than that at night, which is mainly because ET is large in the daytime and small at night [29], and clouds play opposite roles in the land–atmosphere heat fluxes in the daytime and nighttime [30]. Cloud cover reduces downwelling solar radiation in the daytime and emits longwave radiation fluxes at night.

According to Lobell et al. and Yu et al. [53,54], the apparent spatial difference of ICE across the NCP (Figure 5) is related to the local background. In the northern NCP, the additional water from irrigation can significantly increase the soil water content, which greatly affects the local biophysical processes (e.g., air humidity, NDVI, ET, etc.), resulting in noticeable differences in the LST between the humid irrigated areas and adjacent dry non-irrigated areas. In the southern NCP, which experiences more rainfall (Figure S4), the soil moisture is high under natural conditions, rendering the impact of irrigation water on LST weaker than that in the northern NCP. The spatial heterogeneity of the irrigation effects on NDVI, ET, and climate (ΔNDVI, ΔET, ΔTem, and ΔPre, Figure 9) may be one of the reasons for the spatial differences of ICE on LST, because we found that the ICEs were correlated with them (Figure 11). For the marginal areas of the agricultural areas, the irrigation facilities may be imperfect when croplands are remote. In Beijing, a highly modernized city, the widespread use of water-saving irrigation technology has led to a decrease in agricultural water consumption. This can reduce the total ET in the irrigated areas; therefore, the ICEs in these areas were weak or even turned into a warming effect (Figure 5).

In addition, irrigation had a promoting effect on NDVI and ET and an inhibiting effect on Tem and precipitation (Figure 8). This is related to the fact that irrigation promotes crop growth by enhancing the soil moisture and modulates LST and near-surface Tem through energy and water exchange between the surface and atmosphere [10]. The ICE can strengthen the atmosphere's stability, which has a negative influence on the local precipitation [21]. In the interaction of ΔNDVI, ΔET, ΔTem, ΔPre, ERA, and ICE (ΔLST and ΔDCT), we found that ΔET, ΔNDVI, and ΔTem were the main factors driving ICE, and ICE was very sensitive to their changes (Figures 11 and 12). Among them, ΔTem was significantly positively correlated with ΔLST_d and ΔDCT_d, but all of them were significantly negatively correlated with ΔNDVI and ΔET; therefore, the increase in ΔTem in the multiple regression model can also cause the decrease in ΔLST_d and ΔDCT_d (Figure 12). ΔNDVI and ΔET can explain about 20% and 18% of nighttime ICE on average, and they showed a significant trend of 0.003 10 yr^{-1} and −0.23 mm 10 yr^{-1} at yearly scale, respectively; therefore, the increase in ΔNDVI may be one reason why the ICE showed a significant enhancement trend (0.04 °C 10 yr^{-1}) at night from 2000 to 2015 (Figure 4). Spatially, more

than half of the pixels showed an increased ΔNDVI, ΔET, ΔTem, and ΔPre, which may be the cause of more than half of the pixels showing enhanced ICE (Figure 10).

Several limitations of this study need to be addressed. Firstly, due to the lack of reliable dynamic irrigation maps of the NCP at present, the research is based on a static irrigation map. This limits the research on spatiotemporal variation of ICE caused by irrigation expansion and intensity. Secondly, the crop types in the non-irrigated pixels were not distinguished in this study, which may cause biases to our results. To clarify this issue, we compared the LST of mixed non-irrigated crop pixels with that of non-irrigated wheat and corn pixels within the same moving window, respectively. The results show that without distinguishing the crop types, the ICE would be slightly overestimated; however, the biases caused by different crops in non-irrigated areas (about 0.21 and 0.04 °C, Figure TS2 of Text S2 in supplementary material) are much smaller compared to the detected ICE magnitudes (about −0.53 and −0.16 °C, Figure TS2a,d of Text S2) over the irrigated winter wheat and summer corn areas during the growing season. This indicates that the uncertainty caused by different crops is acceptable, and it is unlikely to have had a significant influence on the identified ICE. Thirdly, with the development of water-saving irrigation [55], many water-saving irrigation technologies have emerged, such as sprinkler irrigation, drip irrigation under mulch, etc. Generally, the ET of the same crop is different under different irrigation methods [56], leading to various ICEs. It has been proved that the ICE was attenuated with the large-scale application of water-saving technology in northwest China [12,57]; however, it is difficult to consider the differences in irrigation techniques and irrigation schedules in this study. To further understand the mechanism behind the ICE, researchers should conduct a comprehensive analysis in the future.

5. Conclusions

A novel moving window algorithm was used to identify the irrigation effect on LST, and we used ΔLST and a new index ΔDCT to quantify the ICE on the LST. Based on satellite observations, this study has provided observational evidence that irrigation affected the climate, crop growth, ET, and LST over the NCP from 2000 to 2015. The novel moving window algorithm further eliminated the influence of air temperature on LST. The assessments of the irrigation effect on LST based on ΔLST and ΔDCT were consistent, and ΔDCT had an excellent performance.

Irrigation generally had a cooling effect on LST, and the ICE had apparent spatiotemporal heterogeneity. It was strong in the northern NCP, daytime, and the growing season, especially in spring, whereas it was weak (<0.1 °C) in the southern NCP. In spring, the average ICE was around 0.37 °C and 0.50 °C during the daytime in the NCP and northern NCP, respectively. Irrigation also inhibited precipitation and Tem (-1.461 mm yr^{-1} and -0.023 °C in spring) and promoted ET and NDVI (0.289 mm yr^{-1} and 0.03 in spring). These effects had a similar spatiotemporal heterogeneity to the ICE. The ΔNDVI, ΔET, and ΔTem were the main factors driving the ICE and explained about 22.1–22.8%, 43.8–45.4%, and 25.0–25.9% of ICE_d. For every unit of them increased, the ICE_d enhanced by about 7.2–7.5, 4.5–4.7, and 1.1–1.9 °C, respectively. From 2000 to 2015, more than half of the pixels showed an enhanced ICE; the irrigation effect on nighttime LST and NDVI enhanced significantly (0.04 °C 10 yr^{-1} and 0.003 10 yr^{-1}), but that of ET weakened significantly (0.23 mm 10 yr^{-1}). Our findings provide useful information for studying the effects of irrigation on LST and regional climate. The method provides a new research perspective for quantifying irrigation effects on climate and surface properties, which is more suitable for regions with uneven terrain and climate.

Supplementary Materials: The following supporting information can be downloaded at: https://www.mdpi.com/article/10.3390/rs15184571/s1, Text S1: Sensitivity tests of parameters in the moving window; Text S2: Assess the impact of crop type differences in non-irrigated areas on our result; Figure S1. Effective radiation (ERA) in the North China Plain; Figure S1: Effective radiation (ERA) in the North China Plain; Figure S2: Spatial patterns (a–d) of the average seasonal and annual LST difference (ΔLST_{dem}) between irrigated area and non-irrigated area obtained by the previous

algorithm in the NCP from 2000 to 2015; Figure S3: Temporal patterns of the precipitation (Pre), air temperature (Tem), NDVI, ET, daytime LST (DLST), and nighttime LST (NLST) in irrigated and non-irrigated crop areas of the NCP from 2000 to 2015; Figure S4: Spatial patterns and frequency distributions of the annual average precipitation (Pre), air temperature (Tem), NDVI, ET, daytime and nighttime LST (DLST and NLST) in irrigated and non-irrigated areas of the NCP cropland from 2000 to 2015; Table S1: Differences between ΔLSTdem and ΔLST in the different seasons and administrative districts of the NCP; Table S2: The percentage (%) of the difference between ΔLSTdem and ΔLST in the ΔLST; Table S3: The differences of the annual average irrigation cooling effect (ICE) in the NCP quantified by ΔLST and ΔDCT; Table S4: Difference of the annual average irrigation cooling effect (ICE) in the different administrative districts of the NCP quantified based on ΔLST and ΔDCT. References [32,58,59] are cited in the supplementary materials.

Author Contributions: Methodology, M.H. and L.Z.; Formal analysis, M.H.; Writing—original draft, M.H.; Writing—review & editing, L.Z. and A.L.; Supervision, A.L.; Funding acquisition, L.Z. and A.L. All authors have read and agreed to the published version of the manuscript.

Funding: This research was funded by [National Natural Key Research and Development Program of China] grant number [2019YFE0127600] and [Fundamental Research Funds for the Central Universities] grant number [2042022gf0012]. And The APC was funded by [Fundamental Research Funds for the Central Universities].

Acknowledgments: This paper benefits from data provided by the National Earth System Science Data Center, Geospatial Data Cloud site, and Global Change Research Data Publishing and Repository, National Science and Technology Infrastructure of China, and Resource and Environment Science and Data Center, Chinese Academy of Science.

Conflicts of Interest: The authors declare that they have no known competing financial interest or personal relationships that could have appeared to influence the work reported in this paper.

References

1. Albaladejo-García, J.A.; Alcon, F.; Martínez-Paz, J.M. The Irrigation Cooling Effect as a Climate Regulation Service of Agroecosystems. *Water* **2020**, *12*, 1553. [CrossRef]
2. Li, Y.; Guan, K.; Peng, B.; Franz, T.E.; Wardlow, B.; Pan, M. Quantifying irrigation cooling benefits to maize yield in the US Midwest. *Glob. Chang. Biol.* **2020**, *26*, 3065–3078. [CrossRef] [PubMed]
3. Döll, P. Vulnerability to the impact of climate change on renewable groundwater resources: A global-scale assessment. *Envi-ron. Res. Lett.* **2009**, *4*, 35006. [CrossRef]
4. Shiklomanov, I.A. Appraisal and Assessment of World Water Resources. *Water Int.* **2000**, *25*, 11–32. [CrossRef]
5. Siebert, S.; Burke, J.; Faures, J.M.; Frenken, K.; Hoogeveen, J.; DÖll, P.; Portmann, F.T. Groundwater use for irrigation—A global inventory. *Hydrol. Earth Syst. Sci.* **2010**, *14*, 1863–1880. [CrossRef]
6. Siebert, S.; Döll, P.; Hoogeveen, J.; Faures, J.M.; Frenken, K.; Feick, S. Development and validation of the global map of irriga-tion areas. *Hydrol. Earth Syst. Sci.* **2005**, *9*, 535–547. [CrossRef]
7. Kueppers, L.M.; Snyder, M.A.; Sloan, L.C. Irrigation cooling effect: Regional climate forcing by land-use change. *Geophys. Res. Lett.* **2007**, *34*, L03703. [CrossRef]
8. Guimberteau, M.; Laval, K.; Perrier, A.; Polcher, J. Global effect of irrigation and its impact on the onset of the Indian summer monsoon. *Clim. Dyn.* **2012**, *39*, 1329–1348. [CrossRef]
9. Kang, S.; Eltahir, E.A.B. Impact of Irrigation on Regional Climate Over Eastern China. *Geophys. Res. Lett.* **2019**, *46*, 5499–5505. [CrossRef]
10. Chen, X.; Jeong, S. Irrigation enhances local warming with greater nocturnal warming effects than daytime cooling effects. *Environ. Res. Lett.* **2018**, *13*, 24005. [CrossRef]
11. Li, D.; Chen, Y.; Hu, T.; Cui, Y.; Luo, Y.; Luo, H.; Meng, Q. Climate changes in the Lhasa River basin, Tibetan Plateau: Irriga-tion-induced cooling along with a warming trend. *Theor. Appl. Climatol.* **2020**, *140*, 1043–1054. [CrossRef]
12. Fu, J.; Kang, S.; Zhang, L.; Li, X.; Gentine, P.; Niu, J. Amplified warming induced by large-scale application of water-saving techniques. *Environ. Res. Lett.* **2022**, *17*, 34018. [CrossRef]
13. Douglas, E.M.; Niyogi, D.; Frolking, S.; Yeluripati, J.B.; Roger, A.P.S.; Niyogi, N.; Vörösmarty, C.J.; Mohanty, U.C. Changes in moisture and energy fluxes due to agricultural land use and irrigation in the Indian Monsoon Belt. *Geophys. Res. Lett.* **2006**, *33*, L14403. [CrossRef]
14. Yang, Q.; Huang, X.; Tang, Q. Global assessment of the impact of irrigation on land surface temperature. *Sci. Bull.* **2020**, *65*, 1440–1443. [CrossRef] [PubMed]
15. Boucher, O.; Myhre, G.; Myhre, A. Direct human influence of irrigation on atmospheric water vapour and climate. *Clim. Dyn.* **2004**, *22*, 597–603. [CrossRef]

16. Chen, L.; Dirmeyer, P.A. Global observed and modelled impacts of irrigation on surface temperature. *Int. J. Climatol.* **2019**, *39*, 2587–2600. [CrossRef]
17. Zhu, X.; Liang, S.; Pan, Y.; Zhang, X. Agricultural irrigation impacts on land surface characteristics detected from satellite data products in Jilin province, China. *IEEE J. Sel. Top. Appl. Earth Obs. Remote Sens.* **2011**, *4*, 721–729. [CrossRef]
18. Zhang, C.; Ge, Q.; Dong, J.; Zhang, X.; Li, Y.; Han, S. Characterizing spatial, diurnal, and seasonal patterns of agricultural irri-gation expansion-induced cooling in Northwest China from 2000 to 2020. *Agric. For. Meteorol.* **2023**, *330*, 109304. [CrossRef]
19. Kang, S.; Eltahir, E.A.B. North China Plain threatened by deadly heatwaves due to climate change and irrigation. *Nat. Commun.* **2018**, *9*, 2894. [CrossRef]
20. Li, J.; Chen, Y.D.; Gan, T.Y.; Lau, N. Elevated increases in human-perceived temperature under climate warming. *Nat. Clim. Chang.* **2018**, *8*, 43–47. [CrossRef]
21. Wu, L.; Feng, J.; Miao, W. Simulating the Impacts of Irrigation and Dynamic Vegetation Over the North China Plain on Re-gional Climate. *J. Geophys. Res. Atmos.* **2018**, *123*, 8017–8034. [CrossRef]
22. Zou, Z.; Yang, Y.; Qiu, G. Quantifying the Evapotranspiration Rate and Its Cooling Effects of Urban Hedges Based on Three-Temperature Model and Infrared Remote Sensing. *Remote Sens.* **2019**, *11*, 202. [CrossRef]
23. Zhu, P.; Burney, J. Untangling irrigation effects on maize water and heat stress alleviation using satellite data. *Hydrol. Earth Syst. Sci.* **2022**, *26*, 827–840. [CrossRef]
24. Xiao, L.; Asseng, S.; Wang, X.; Xia, J.; Zhang, P.; Liu, L.; Tang, L.; Cao, W.; Zhu, Y.; Liu, B. Simulating the effects of low-temperature stress on wheat biomass growth and yield. *Agric. For. Meteorol.* **2022**, *326*, 109191. [CrossRef]
25. Karimzadeh Soureshjani, H.; Ghorbani Dehkordi, A.; Bahador, M. Temperature effect on yield of winter and spring irrigated crops. *Agric. For. Meteorol.* **2019**, *279*, 107664. [CrossRef]
26. Makowski, D.; Marajo-Petitzon, E.; Durand, J.; Ben-Ari, T. Quantitative synthesis of temperature, CO2, rainfall, and adaptation effects on global crop yields. *Eur. J. Agron.* **2020**, *115*, 126041. [CrossRef]
27. Bonfils, C.; Lobell, D. Empirical evidence for a recent slowdown in irrigation-induced cooling. *Proc. Natl. Acad. Sci. USA* **2007**, *104*, 13582–13587. [CrossRef]
28. Gao, K.; Santamouris, M.; Feng, J. On the cooling potential of irrigation to mitigate urban heat island. *Sci. Total Environ.* **2020**, *740*, 139754. [CrossRef]
29. Lobell, D.B.; Bonfils, C.J.; Kueppers, L.M.; Snyder, M.A. Irrigation cooling effect on temperature and heat index extremes. *Ge-ophys. Res. Lett.* **2008**, *35*, L09705. [CrossRef]
30. Cook, B.I.; Shukla, S.P.; Puma, M.J.; Nazarenko, L.S. Irrigation as an historical climate forcing. *Clim. Dyn.* **2015**, *44*, 1715–1730. [CrossRef]
31. Shiflett, S.A.; Liang, L.L.; Crum, S.M.; Feyisa, G.L.; Wang, J.; Jenerette, G.D. Variation in the urban vegetation, surface temper-ature, air temperature nexus. *Sci. Total Environ.* **2017**, *579*, 495–505. [CrossRef]
32. Yang, Q.; Huang, X.; Tang, Q. Irrigation cooling effect on land surface temperature across China based on satellite observa-tions. *Sci. Total Environ.* **2020**, *705*, 135984. [CrossRef]
33. Liu, G.; Wang, W. Irrigation-Induced Crop Growth Enhances Irrigation Cooling Effect Over the North China Plain by In-creasing Transpiration. *Water Resour. Res.* **2023**, *59*, e2022WR034142. [CrossRef]
34. Liu, G.; Wang, W.; Shao, Q. Recent Decline of Irrigation-Induced Cooling Effect Over the North China Plain in Observations and Model Simulations. *Geophys. Res. Lett.* **2023**, *50*, e2022GL101973. [CrossRef]
35. Coll, C.; Wan, Z.; Galve, J.M. Temperature-based and radiance-based validations of the V5 MODIS land surface temperature product. *J. Geophys. Res.* **2009**, *114*, D20102. [CrossRef]
36. Duan, S.; Li, Z.; Li, H.; Göttsche, F.; Wu, H.; Zhao, W.; Leng, P.; Zhang, X.; Coll, C. Validation of Collection 6 MODIS land sur-face temperature product using in situ measurements. *Remote Sens. Environ.* **2019**, *225*, 16–29. [CrossRef]
37. Wan, Z. New refinements and validation of the collection-6 MODIS land-surface temperature/emissivity product. *Remote Sens. Environ.* **2014**, *140*, 36–45. [CrossRef]
38. Zhang, Z.; Lin, A.; Zhao, L.; Zhao, B. Attribution of local land surface temperature variations response to irrigation over the North China Plain. *Sci. Total Environ.* **2022**, *826*, 154104. [CrossRef]
39. Jackson, R.D.; Idso, S.B.; Reginato, R.J.; Pinter, J.P.J. Canopy temperature as a crop water stress indicator. *Water Resour. Res.* **1981**, *17*, 1133–1138. [CrossRef]
40. Balota, M.; Payne, W.A.; Evett, S.R.; Peters, T.R. Morphological and physiological traits associated with canopy temperature depression in three closely related wheat lines. *Crop Sci.* **2008**, *48*, 1897–1910. [CrossRef]
41. Hou, M.; Tian, F.; Zhang, T.; Huang, M. Evaluation of canopy temperature depression, transpiration, and canopy greenness in relation to yield of soybean at reproductive stage based on remote sensing imagery. *Agric. Water Manag.* **2019**, *222*, 182–192. [CrossRef]
42. Xiao, D.X.D.; Tao, F.T.F. Contributions of cultivars, management and climate change to winter wheat yield in the North China Plain in the past three decades. *Eur. J. Agron.* **2014**, *52*, 112–122. [CrossRef]
43. Zhao, Z.A.; Qin, X.A.; Wang, Z.A.; Wang, E.B. Performance of different cropping systems across precipitation gradient in North China Plain. *Agric. For. Meteorol.* **2018**, *259*, 162–172. [CrossRef]
44. Meng, Q.; Sun, Q.; Chen, X.; Cui, Z.; Yue, S.; Zhang, F.; Rmheld, V. Alternative cropping systems for sustainable water and nitrogen use in the North China Plain. *Agric. Ecosyst. Environ.* **2012**, *146*, 93–102. [CrossRef]

45. Peng, S.; Ding, Y.; Liu, W.; Li, Z. 1 km monthly temperature and precipitation dataset for China from 1901 to 2017. *Earth Syst. Sci. Data* **2019**, *11*, 1931–1946. [CrossRef]
46. Cao, W.; Duan, C.; Yang, T.; Liu, R. Daily surface effective radiation at 130 radiation stations in China (1971–2014) [J/DB/OL]. *Digital J. Glob. Chang. Data Repository* **2018**. [CrossRef]
47. Meier, J.; Zabel, F.; Mauser, W. A global approach to estimate irrigated areas-a comparison between different data and statis-tics. *Hydrol. Earth Syst. Sc.* **2018**, *22*, 1119–1133. [CrossRef]
48. Kumar, S.; Dirmeyer, P.A.; Merwade, V.; DelSole, T.; Adams, J.M.; Niyogi, D. Land use/cover change impacts in CMIP5 climate simulations: A new methodology and 21st century challenges. *J. Geophys. Res. Atmos.* **2013**, *118*, 6337–6353. [CrossRef]
49. Zhao, N.; Han, S.; Xu, D.; Wang, J.; Yu, H. Cooling and Wetting Effects of Agricultural Development on Near-Surface Atmos-phere over Northeast China. *Adv. Meteorol.* **2016**, *2016*, 6439276. [CrossRef]
50. Cook, B.I.; Puma, M.J.; Krakauer, N.Y. Irrigation induced surface cooling in the context of modern and increased greenhouse gas forcing. *Clim. Dyn.* **2011**, *37*, 1587–1600. [CrossRef]
51. Zhang, X.; Xiong, Z.; Tang, Q. Modeled effects of irrigation on surface climate in the Heihe River Basin, Northwest China. *J. Geophys. Res. Atmos.* **2017**, *122*, 7881–7895. [CrossRef]
52. Nishida, K.; Yoshida, S.; Shiozawa, S. Theoretical analysis of the effects of irrigation rate and paddy water depth on water and leaf temperatures in a paddy field continuously irrigated with running water. *Agric. Water Manag.* **2018**, *198*, 10–18. [CrossRef]
53. Lobell, D.; Bala, G.; Mirin, A.; Phillips, T.; Maxwell, R.; Rotman, D. Regional Differences in the Influence of Irrigation on Cli-mate. *J. Clim.* **2009**, *22*, 2248–2255. [CrossRef]
54. Yu, Z.; Xu, S.; Zhang, Y.; Jørgensen, G.; Vejre, H. Strong contributions of local background climate to the cooling effect of ur-ban green vegetation. *Sci. Rep.* **2018**, *8*, 6789.
55. Qu, S.; Wang, L.; Lin, A.; Zhu, H.; Yuan, M. What drives the vegetation restoration in Yangtze River basin, China: Climate change or anthropogenic factors? *Ecol. Indic.* **2018**, *90*, 438–450. [CrossRef]
56. Hou, M.; Tian, F.; Zhang, L.; Li, S.; Du, T.; Huang, M.; Yuan, Y. Estimating Crop Transpiration of Soybean under Different Ir-rigation Treatments Using Thermal Infrared Remote Sensing Imagery. *Agronomy* **2019**, *9*, 8. [CrossRef]
57. Zhang, C.; Dong, J.; Leng, G.; Doughty, R.; Zhang, K.; Han, S.; Zhang, G.; Zhang, X.; Ge, Q. Attenuated cooling effects with increasing water-saving irrigation: Satellite evidence from Xinjiang, China. *Agric. For. Meteorol.* **2023**, *333*, 109397. [CrossRef]
58. Lei, H. Distribution maps of crop planting areas in the North China Plain (2001–2018). *Natl Tibetan Plateau Data Center* **2022**. [CrossRef]
59. Li, J.; Lei, H. Tracking the spatio-temporal change of planting area of winter wheat-summer maize cropping system in the North China Plain during 2001–2018. *Comput. Electron. Agric.* **2021**, *187*, 106222. [CrossRef]

Disclaimer/Publisher's Note: The statements, opinions and data contained in all publications are solely those of the individual author(s) and contributor(s) and not of MDPI and/or the editor(s). MDPI and/or the editor(s) disclaim responsibility for any injury to people or property resulting from any ideas, methods, instructions or products referred to in the content.